U.PORTO
INSTITUTO DE CIÊNCIAS BIOMÉDICAS ABEL SALAZAR
UNIVERSIDADE DO PORTO

U.PORTO
FEUP FACULDADE DE ENGENHARIA
UNIVERSIDADE DO PORTO

**Miguel Diogo de Freitas Horta**

# Design and development of novel magnetic lipid nanoparticles for anti-cancer therapy

**Supervisor: Prof. Dr. Salette Reis**
**Co-supervisor: Dr. Cláudia Nunes**

**Mestrado Integrado em Bioengenharia**
**Faculty of Engineering of University of Porto**
**September 2015**

**-This page was intentionally left blank.-**

# Abstract

Cancer is the third leading cause of worldwide morbidity, only surpassed by cardiovascular and infectious diseases. Nonetheless, and despite all the efforts being made, humanity is as far away from real progress in fighting this pathology as it was decades ago. Nanotechnology has appeared as a hopeful partner in this battle, in that it has introduced new ways to improve the current therapies based in antineoplastic drugs. These drugs, which were in desperate need of improvement, tend to kill almost as much as the disease itself, through their aggressive systemic side effects.

Among nanotechnology's tools for such improvements are nanostructured lipid carriers (NLC) and superparamagnetic iron oxide nanoparticles (SPION). NLCs are biocompatible nanometric sphere-like meshes of lipids which have the ability to encapsulate drugs within its pores, travel through the blood stream undetected (when below 200 nanometers), slowly and controllably release the contained drug and deliver it to, and only to, the target location. A magnitude smaller, SPIONs are an agglomeration of iron oxides, usually in a sphere shape, very prone to modulation. They can perform a plethora of accomplishments, ranging from diagnostics to therapeutics and even both at the same time.

This thesis followed a three-pronged approach, and is thus divided as such. First and foremost, a paclitaxel-loaded NLC formulation was optimized through an iterative process. The final iteration yielded a spherical nanoparticle suspension with 117.83 nm of average diameter, a ζ-potential of -29.2 mV, polydispersity index of 0.113 and encapsulation efficiency higher than 99%, which was then used as a stepping stone for the third section of this work. Secondly, a fast, reliable and reproducible synthesis methodology for SPIONs was designed, developed, optimized and characterized. The developed process was based in a microwave-assisted method and resulted in crystalline iron oxide nanoparticles with a near-null coercivity, in a somewhat broad range of diameters (5-15 nm) with a few multi-domain outliers. The possible existence of a thin maghemite coating was not ruled out, as there was evidence of strong interparticle dipolar interactions. In the last section, a paclitaxel-SPION-loaded NLC formulation was optimized through a Box-Behnken experimental design and characterized. The chosen formulation was synthesized with a ratio of solid to liquid lipid of 7, 10 mg of paclitaxel and a 15 minutes sonication time. It resulted in a 94.9 nm NLC with 0.165 of polydispersity index, encapsulation efficiency (of paclitaxel) of 81.14% and a -29.2 mV ζ-potential. SQUID and XRD measurements confirmed the SPIONs' presence inside the NLCs. The formulation showed a slow and uncharacteristic release profile, withholding three quarters of the encapsulated paclitaxel for more than 68 hours, while releasing more quantity in a simulated neoplastic environment.

# Resumo

O cancro é atualmente a terceira causa de morte em todo mundo, sendo apenas ultrapassado por doenças cardiovasculares e infeciosas. Mesmo apesar de vários esforços estarem a ser feitos, a Humanidade está tão longe de atingir avanços na erradicação da doença como estava há décadas atrás. A nanotecnologia surge como um novo parceiro nesta batalha, no sentido em que possibilita melhorar as atuais terapias baseadas em fármacos antineoplásicos, os quais necessitam desesperadamente de aperfeiçoamento uma vez que tendem a matar quase tanto como a própria doença, através dos seus efeitos secundários agressivos e sistémicos.

Entre as diversas nanopartículas que são hoje possível sintetizar encontram-se os transportadores lipídicos nanoestruturados (TLN) e as nanopartículas superparamagnéticas de óxido de ferro (NSOF). Os TLN são esferas lipídicas biocompatíveis, que têm a capacidade de encapsular fármacos, percorrer a corrente sanguínea sem serem detetados (desde que tenham menos de 200 nm), libertar o fármaco contido de forma lenta e controlada e entregá-lo a apenas um local-alvo. De um tamanho cerca de dez vezes menor, as NSOF são aglomerados de óxidos de ferro, comumente esféricos, facilmente modulados. Podem ter várias aplicações biomédicas desde diagnósticos até terapias, ou mesmo ambos simultaneamente.

Esta tese é o resultado de uma abordagem a três vertentes, e está dividida como tal. Primeiramente, várias formulações de TLNs contendo paclitaxel foram desenvolvidas por forma a se chegar a uma formulação otimizada, através de um processo iterativo. A iteração final resultou numa suspensão de nanopartículas esféricas com 118 nm de diâmetro, um potencial-ζ de -29.2 mV, índice de polidispersão de 0.113 e uma eficiência de encapsulação maior que 99%, a qual foi então utilizada como base para a terceira secção deste trabalho. Em segundo lugar, foi desenhada, desenvolvida, otimizada e caracterizada uma metodologia para a síntese de NSOFs que fosse rápida, reproduzível e de confiança. O processo desenvolvido foi baseado num método assistido por micro-ondas e resultou em nanopartículas de óxido de ferro cristalinas com uma coercividade quase nula à temperatura ambiente, com um intervalo de diâmetros um pouco largo (5-15 nm), o que poderá indicar a existência algumas partículas com mais de um domínio magnético. A possível existência de uma fina camada de maghemite na superfície não foi desconsiderada, na medida em que se identificou uma forte interação entre partículas de natureza dipolar. Na última secção, uma formulação de TLN contendo paclitaxel e NSOF foi produzida e otimizada através de um desenho experimental do tipo Box-Behnken, tendo-se procedido também à sua caracterização. A formulação escolhida foi sintetizada com um rácio de lípido sólido para líquido de 7, 10 mg de paclitaxel e um tempo de sonicação de 15 minutos. O resultado final foi uma formulação com um diâmetro médio de 95 nm com 0.165 de índice de polidispersão, eficiência de encapsulação (de paclitaxel) de 81.1% e -29.2 mV de potencial-ζ. Medidas de SQUID e difração de raios X confirmaram a presença das NSOF dentro das TLNs. A formulação demonstrou possuir um perfil de libertação de fármaco lento e em dois regimes distintos, retendo três quartos do paclitaxel encapsulado durante mais de 68 horas e libertando maior quantidade no ambiente de simulação de cancro.

# Acknowledgements

First and foremost, I would like to thank Professor Salette Reis for this wonderful learning opportunity. Thank you for accepting me, teaching me and sometimes guiding me, for all the little chats and funny stories in the balcony and, in general, thank you for the past six months.

To Doctor Cláudia Nunes, I send the most sincere of thank yous. I know sometimes you thought you weren't helping me enough (I bet these last few days turned that thought around) but you did. Not just a little bit either. You see, the time we spent together was not solely science. Of course, you taught me enough science to write a few of these thesis. But you did so much more. Because of you, your help and your attitude in life and work, I know I became a better person and a better scientist (well, isn't that a cliché). I arrived loving science, and I'll leave loving it more. I know I wasn't the easiest person to pass through your hands (procrastination comes to mind) but I'll bet I was the one who liked it the most. So thank you, for everything.

Next, a great deal of gratitude to my whole family, especially my mother and father. For all the hard work you did during 22 years. For all the support and for believing, well, most of the times at least, that I would graduate in 5 years. I kid, I know you had no doubts. Look at the fruits of your labor. It's starting to pay off!

To Inês, for staying by my side for so long and enduring so much. All my heart (well, except the bits that went for the last paragraph) goes to you.

Afterwards, a big hug to my lab mates. Trust me girls, I'm doing this in a random order. You can bet it wouldn't have been the same without you all. To Catarina Alves, for all the tidbits of advice and companionship, and for keeping me grounded. It seems I can't make a living out of patents. Shame. To Mara, for teaching me the beauty and usefulness of the ultrasound. This thesis would have taken a couple more days to finish hadn't been for her. And the crosswords. Good times. To Joaninha, for all the companionship she offered, and for the readiness she accepted me as I entered the workspace. To Virgínia, for alerting me about the number of burger houses there are. There really is a big number of them in this town. To Catarina PL, for the quickness of advice whenever it was needed. To Alexandre (sorry about the girls part at the start) and Luise for being so available. And to Nini, for scheduling my DLS. It is you, who made all my work possible, especially the size measurement parts!

Lastly, to all my friends, both old and new, from kindergarten to college, for simply being there. And to Nhetas! We had some good 5 years, didn't we?

Alas, a thank you all around. I appreciated getting acquainted to all of you. We'll keep in touch.

# Index

# Figure list

# Table list

# Chapter 1

## Nanotechnology in medicine

Nanotechnology represents the field of sub-micron manipulation, which allows to assemble and control particles of 1/80000$^{th}$ the size of the average human hair [1]. As the particle size diminishes, its physicochemical properties and environmental interactions begin to change, largely due to increased surface area to volume ratio. Nanoparticles can be seen as a bridge between the macroscopic world ruled by classical physics and the atomic world, ruled by quantum physics.

Although it may seem a futuristic science, nanotechnology has emerged over 40 years ago, with Gerd Birrenbach's attempt at a process he called "micelle polymerization" in 1969 [2]. Since then, research on nanoparticles has increased exponentially (**Figure 1**).

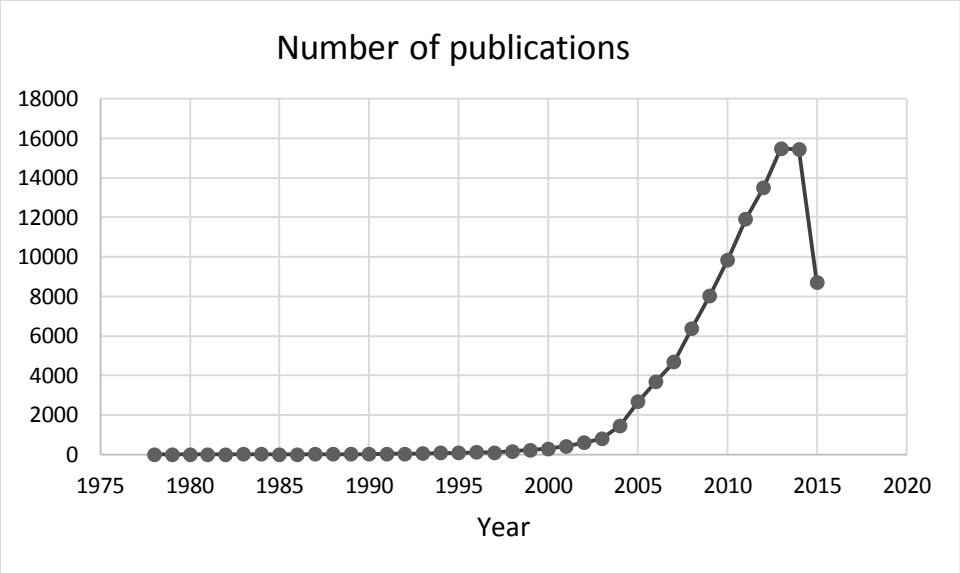


***Figure 1.*** Graphical representation of the number of articles published in Pubmed during the last 35 years. Information collected on 2015, July 7th.

One of the fields most responsible for this accelerated growth is nanomedicine, the therapeutic and diagnostic field of nanotechnology.

Among the therapeutic applications, the most frequently employed revolve around utilizing nanoparticles as delivery agents, which act as vehicles for drugs [3-5], heat releasing [6, 7] or light emitting molecules [8] allowing them to reach specific types of cells or extracellular locations. These nanoparticles are engineered in such a way that they are attracted to a specific environment, allowing a directed treatment and, therefore, reducing the therapeutic agent's

damage to bystander cells. Other less used nanotherapy techniques have also been reported, such as nanosponges, polymeric nanoparticles coated with a red blood cell membrane which act as decoys and intercept toxins in the blood stream [9] or a lens coated with carbon nanotubes which can convert light to tightly focused sound waves [10], among a multitude of others.

Due to the high diversity among different nanoparticle types, they can be applied to any of the existing diagnostic techniques, frequently increasing their efficiency, both in output velocity and quality. The most commonly known application lies in Magnetic Resonance Imaging (MRI), where superparamagnetic iron oxides coated with a recognition molecule, such as a tumor-binding molecule, provide a localized contrast [11]. Another use of nanoparticles in diagnostic involves an encapsulation or functionalization with a fluorescent molecule, allowing an optical detection [12]. There are also reports of multimodal nanoparticles which comprise both of the previous functions [13]. In a simpler approach, semiconductor nanoparticles known as quantum dots have been extensively studied due to their unique physiochemical properties, conferred by a quantum confinement effect [14], allowing for varied applications such as molecule tracking [15] and fluorescence imaging [16].

Aside from imaging techniques, most applications can be classified as nanosensors. A sensor, by definition, recognizes an agent and consequently produces a signal. In nanodiagnostics, the detection is based on the recognition of a specific molecule or a change in the environment and the signal can range from an absorbance shift due to agglomeration [17], to a release of light [18], or a magnetic resonance change [19].

In the present decade, a more condensed and multifunctional strategy has surfaced, called theranostics, combining both diagnostic and therapy in a single agent. The purpose is to diagnose and treat the disease at its earliest stage, improving the likelihood of a cure. Nanoparticles are excellent candidates for this approach due to their high variability and modification possibilities [20]. All types of nanoparticles can be engineered to achieve such a goal, being them organic, inorganic or even a combination of both [21-24].

A somewhat recent review (2013) on the current state of nanomedicine showed that most approved and investigated products on this field are categorized by the U.S. Food and Drug Administration as drug nanocarriers, more than 80% of which are intended for cancer treatment [25]. It is therefore obvious the existence of a keen oncological interest by today's population of "nanoresearchers".

# Nanomedicine in Cancer

The World Health Organization attributed 8.2 million worldwide deaths to cancer in the year of 2012, approximately 13% of all reported deaths, with a 70% estimated increase of cancer cases in the next two decades [26]. One of the main reasons for such high numbers is the lack of efficient treatment. Current antineoplastic agents have poor selectivity, which, in practice, corresponds to a dose-limiting toxicity and systemic action, i.e. either the drug is in a too low concentration, resulting in death by cancer progression, or too high, resulting in the death of healthy cells by drug toxicity. In some cases, the drug concentration could actually be the same in both situations. Alas, the need for a targeted delivery of said drugs is of paramount importance to overcome current oncological treatments' limitations and allow the patient to

outlast its illness, to which nanotechnology responded. Nanoparticles have the potential to increase a drug's *in vivo* stability, extend its blood circulation time, control its release and alter its biodistribution, through either passive or active targeting, essentially allowing for a controlled modulation of the drug's pharmacokinetic and pharmacodynamics profiles.

In **Table 1** are summarized the approved nanoparticles for cancer therapy, evidencing the focus on liposome-type formulations.

***Table 1.*** *Marketed and approved nanoparticles for cancer therapy applications.*

| Product (Company) | Vehicle | Drug | Indication | Approval | Ref. |
|---|---|---|---|---|---|
| DaunoXome® (Galen) | Liposome | Daunorubicin | Kaposi's sarcoma | 1996 | [27] |
| DepoCyt® (Pacira) | Liposome | Cytarabine | Neoplastic meningitis | 1999 | [28] |
| Doxil® Caelyx® (Johnson & Johnson) | Liposome | Doxorubicin | Kaposi's sarcoma Ovarian and breast cancer Multiple myeloma | 1995, 1999, 2003 and 2007 | [29] |
| Genexol-PM® (Samyang Biopharm) | PEG-PLA polymeric micelle | Paclitaxel | Breast, lung and ovarian cancer | 2007 | [30] |
| Lipo-Dox® (Taiwan Liposome) | Liposome | Doxorubicin | Kaposi's sarcoma Breast and ovarian cancer | 1998 | [31] |
| Marqibo® (Talon) | Liposome | Vincristine | Acute lymphoid leukemia | 2012 | [32] |
| Mepact® (Takeda) | Liposome | Mifarmutide | Osteosarcoma | 2009 | [33] |
| Myocet® (Cephalon) | Liposome | Doxorubicin | Breast cancer (in conjunction with cyclophosphamide) | 2000 | [34] |
| NanoTherm® (Magforce Nanotechnologies) | Iron oxide nanoparticle | None[1] | Glioblastoma | 2010 | [35] |

[1] *Intended purpose is thermal ablation instead of drug vehicularization.*

The United States clinical trials registry contains, as of September of 2015, 1620 registries under the keyword "liposome" and 206 under "nanoparticle", which, when compared to the previously listed nine formulations, indicate a growing trend in nanotechnological approaches to cancer therapies.

# Objectives and reasoning

The elaborated thesis encompassed several objectives, which can be grouped into three different sections.

Current pharmaceutical treatments for neoplasms are mostly based on extremely hydrophobic drugs. Such compounds have stability issues in the blood stream and require third-party molecules, known as excipients, to function. Additionally, they have lack of selectivity, affecting both healthy and diseased tissue alike. In this sense, the first objective was to design and develop a Paclitaxel-loaded nanostructured lipid carrier (NLC) formulation. Paclitaxel was chosen due to its degree of hydrophilicity, which is one of the highest known to drugs, representing the ideal experimental subject. The lipid matrix of NLCs confers the perfect environment for Paclitaxel's presence, while their surfactant-stabilized surface would hypothetically permit a very high and long-term stability in aqueous media. Additionally, and perhaps most importantly, they may confer occlusion and bar the Paclitaxel's destructive potential until it reaches its target destination – tumoral tissue.

Magnetic nanoparticles have been establishing an ever-increasing ground in nanomedicine. Albeit more present in diagnostics, they have a wide range of therapeutic capabilities. However, their current commercialization is deficient, largely due to morose and inefficient largescale synthesis methodologies. Such leads to the second objective of this thesis, the development, optimization and characterization of superparamagnetic iron oxide nanoparticles (SPIONS). SPIONs were chosen as focus due to a plethora of reasons. First and foremost, they are comprised of solely iron, a material widely known as biocompatible (in sensible quantities). Secondly, SPIONs are abundant in the scientific literature, with well-described and extensive characterizations, and are already clinically approved and marketed (such as Feridex [36], Feraheme [37] and MION-46L [38]). Thirdly, the reagents needed for their synthesis are cheap and easily acquired and a functioning protocol for their synthesis would be a useful asset to the laboratory. Furthermore, their superparamagnetic behavior confers hyperthermic capabilities - an increase of energy, dissipated as heat, caused by an applied alternated magnetic field.

The thesis's third and ultimate objective consisted on the innovative combination of both previous sections with the intention of creating a synergistic behavior. The synthesis and characterization of this novel formulation, the Paclitaxel-SPION-loaded NLCs, could lead into insights about unexplored reaches of nanotherapeutics and, ideally, result in a massive advance of the drug's effectiveness.

# Chapter 2

## Lipid nanoparticles

### Introduction

Lipid nanoparticles are defined as sub-micron sphere-like arrangements of lipid-based molecules held together by a surfactant. Due to its unique composition, these particles usually attain GRAS (*generally recognized as safe*) status, since its components are biomolecules commonly found in the human body or known to be biocompatible [39].

Currently, this classification encompasses many different types of nanoparticles depending on composition and synthesis method, albeit only two are mainly developed and studied, solid lipid nanoparticles (SLNs) and nanostructured lipid carriers (NLCs).

First developed during the early 1990s [40], SLNs are composed of 0.1-30% (w/w) solid lipid dispersed in an aqueous solution of 0.5-5% (w/w) surfactant [41]. These nanoparticles tend to exhibit a good physicochemical stability, protection and controlled release of the encapsulated drug, low cytotoxicity, organic solvent free synthesis and an ease of scale-up [39]. However, due to their high crystallinity and ordered matrix (**Figure 2.A**), they can suffer from low encapsulation efficiency and a possible drug expulsion during storage [42], depending on the structure of the drug.

To circumvent such limitations, a second generation of lipid nanoparticles was developed. The addition of a liquid lipid to the formulation allows a less ordered lipid matrix and, consequently, more room for the active compound (**Figure 2.B**) [43].

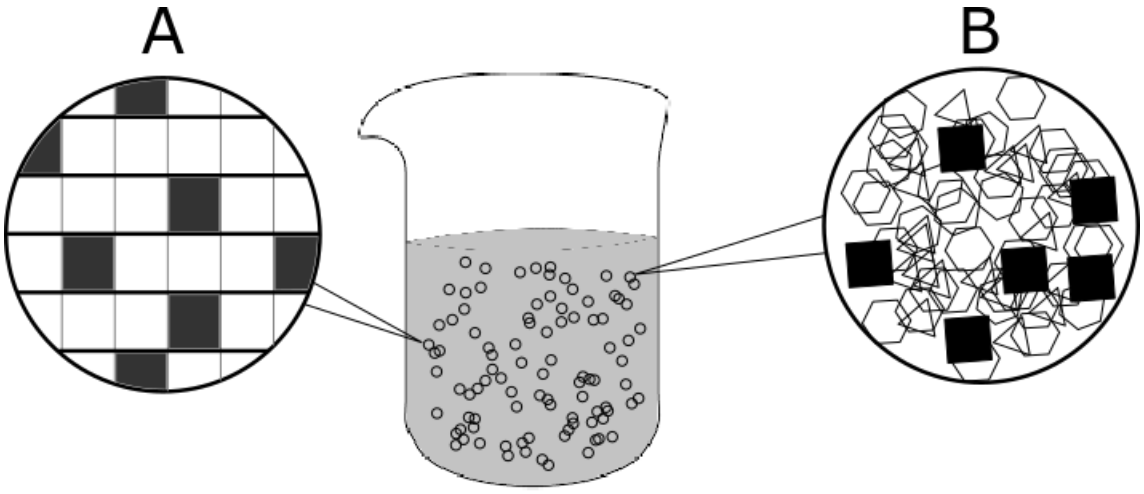


***Figure 2.*** *Lipid matrix representation of solid lipid nanoparticles (A) and nanostructured lipid carriers (B).*

These types of nanoparticles have shown great potential in cancer treatment research. Albeit none is already approved or in ongoing clinical trials, numerous *in vitro* and animal models assays have been conducted successfully and reported in the literature. A very succinct fraction of which is shown in **Table 2**.

***Table 2.*** *Small sample of lipidic nanoparticles' research in cancer therapy.*

| Vehicle | Surface modification | Drug | Cancer type | Reference |
|---|---|---|---|---|
| NLC | Pegylation | 10-hydroxycamptothecin | Lung adenocarcinoma | [44] |
| NLC | - | Celecoxib | Non-small cell lung cancer | [45, 46] |
| NLC | - | Tamoxifen | Breast cancer | [47] |
| NLC | Layer-by-layer polyelectrolyte and pegylation | Doxorubicin | Lung adenocarcinoma and breast cancer | [48] |
| NLC | - | Zerumbone | Acute lymphoblastic leukemia | [49] |
| NLC | Hyaluronic acid | Baicalein and doxorubicin | Breast cancer | [50] |
| NLC | - | Thymoquinone | Breast and cervical cancer | [51] |
| NLC | Hyaluronic acid | 5-fluorouracil and cisplatin | Gastric cancer | [52] |
| NLC | - | Curcumin | Brain cancer | [53] |
| NLC | Enoxolone | Curcumin | Liver cancer | [54] |
| NLC | Folate-poly(PEG-cyanoacrylate-co-cholesteryl cyanoacrylate) copolymer | Docetaxel | Unspecified mouse tumor | [55] |
| NLC | Hyaluronic acid | Paclitaxel | Melanoma and colon carcinoma | [56] |
| SLN | - | Docetaxel | Breast cancer | [57] |
| SLN | - | Resveratrol | Brain cancer | [58] |
| SLN | - | Etoposide | Melanoma metastasis in lung | [59] |
| SLN | Transferrin | Doxorubicin and enhanced green fluorescence protein plasmid | Lung adenocarcinoma | [60] |
| SLN | Pegylated peptide | Paclitaxel | Fibrosarcoma, lung carcinoma | [61] |
| SLN | - | Butyrate | Promyelocytic leukemia | [62] |
| SLN | - | Camptothecin | Brain cancer | [63] |
| SLN | - | Docetaxel and conjugate of folic acid and oxidized | Liver cancer | [64] |

| | | | | |
|---|---|---|---|---|
| | | single-walled carbon nanotubes | | |
| SLN | Hyaluronic acid | Vorinostat | Tongue squamous cell carcinoma and lung adenocarcinoma | [65] |
| SLN | Folic acid | Docetaxel and ketoconazole | Brain endothelioma | [66] |

## Paclitaxel

Paclitaxel, as well as the other taxanes, acts by decreasing the critical concentration of tubulin needed for microtubule assembly, promoting its formation and hindering its detachment [67]. This destabilization of functional microtubule dynamics leads to the impossibility of some essential cell processes, such as movement, chromosome segregation and cell division, ultimately resulting in the cell's unrest and self-induced apoptosis [68].

Along with his structural cousin docetaxel, paclitaxel (**Figure 3**) is the highlight of the taxane family. His tetracyclic heptadecane skeleton confers a staggeringly low hydrophilicity, which was reported to be as low as 0.357 µg/mL [69]. In fact, its behavior in aqueous media lead to the addition of third party molecules, as excipient or binder, as the only method to stabilize this taxoid, with the examples of the two most important marketed forms of paclitaxel, Taxol®, where it is dissolved in a 50/50 (w/w) solution of polyoxyethylated castor oil (Cremophor EL - CrEl) and dehydrated ethanol [70], and Abraxane®, in which the taxoid molecule is conjugated to albumin (nab-paclitaxel) [71].

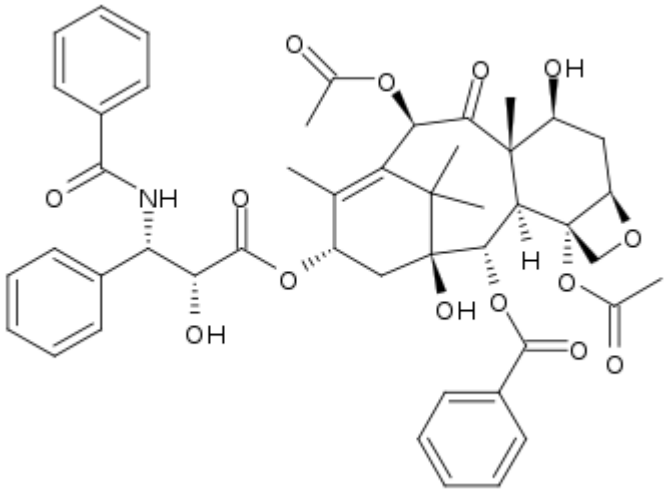


***Figure 3.*** *Paclitaxel structural and chemical configuration.*

The first of the previously enunciated formulations is largely accompanied by undesired pharmacokinetic profiles, due to paclitaxel's extensive binding to serum albumin, and consequent inactivity [72], broad tissue distribution, albeit incapable of passing the blood-brain

barrier [73], and a low half-life of 2.9 ±0.3 hours [74]. Additionally, the excipient CrEl only worsens such effects [75].

The second formulation, on the other hand, demonstrates an increased treatment response and slower disease progression with a simultaneous significantly decreased systemic toxicity [76]. It requires, however, recombinant albumin for its synthesis, relating into a much higher cost and, consequently, turning the better antitumor efficacy relatively marginal.

Nano-sized delivery systems have therefore attracted a heightened attention in the current millennium as a strategy to overcome the limitations of simpler paclitaxel therapy approaches.

Firstly, a nanoparticle system would provide physical and chemical protection for the very water insoluble and metabolic degradation-prone molecule through its entrapment, allowing a higher injectable concentration and completely removing the excipient's presence and toxicity. Secondly, nano-based formulations could improve the paclitaxel's pharmacokinetics through drug occlusion (lack of epitopes recognizable by the immune system), a controlled release profile and possible surface modification (such as pegylation). Thirdly, a nanoparticle can take advantage of the Enhanced Permeation and Retention effect (EPR), a passive targeting approach where small particle (less than circa 400 nanometers) accumulate in cancer tissue through defective neo-angiogenic blood vessels [77], or it can be modulated into partaking an active targeting, with molecules such as folic acid, transferrin and hyaluronic acid. Both the previous targeting methods result in an improved biodistribution of the anticancer agent. Finally, the nano-sized systems have a limitless potential in versatility and functionality modulation. They allow for co-delivery of multiple agents, being it synergistic drugs, a theranostics combination or anything else. They can also be positively, neutral or negatively charged, depending on which suits the synthesizer needs. Environment responses are also possible, such as a pH-, heat-, light- or magnetically-responsive structural change.

A myriad lipid-based nanoparticles have already been reported to effectively deliver paclitaxel.

Liposomal formulations encapsulating paclitaxel have showed a steep decrease in side effects while maintaining a similar to slightly higher antitumor activity when compared to Taxol® [78-80] and even managed to show a significant tumor inhibition in a Taxol®-resistant murine model [81]. Liposomes, however, contain an aqueous core, leading to disappointing encapsulation efficiencies of hydrophobic drugs such as paclitaxel.

On the other hand, SLNs are composed of a solely lipid matrix, more easily accommodating such drugs, leading to higher encapsulation efficiencies and slower release profiles, as has been reported by Cavalli et al (0.1% release in PBS during 2 hours [82]), Yegin et al (12.5-16.5% within 14 days [83]) and Lee at al (10% in 24 hours [84]). The *in vitro* cellular uptake and cytotoxicity has also been shown to be influenced by the lipid matrix composition and surfactant [85-87], which is most likely explained by specific affinities of cell membranes to different lipids. Dong et al presented a clever use of surfactant (Brij 78) which provoked a temporary reduction in intracellular ATP levels partially inhibiting the energy-dependent P-gp efflux (a drug efflux mechanism that some tumors employ) in a P-gp overexpressing human ovarian carcinoma cell line, effectively bypassing its drug resistance. An unexpected find revealed the propensity of SLNs to deliver paclitaxel to the brain, passing through the blood-brain barrier without an active mediator [88].

As stated in the previous chapter, the SLNs' matrix confers potential disadvantage issues, which NLCs were developed to resolve. However, being the most recent addition to the lipid-based nanoparticle family, the reports of successful paclitaxel-loaded NLC formulations are staggeringly scarce. As of the time of writing, the author could only locate five divulged papers on the subject [56, 89-92], three written by the same authors. Yang et al developed started with the development of hyaluronic acid-coated NLC formulation and reported its higher effectiveness in murine melanoma, mouse colon and human colon cancer cell lines, and *in vivo* in Kumming mice when compared to Taxol® [56]. They later went on to disregard the hyaluronic acid and include a surface modification of a photo-responsive cell-penetrating peptide and again reported a higher antitumor efficacy against non-functionalized NLCs and Taxol®, this time in human fibrosarcoma cells [89]. More recently, in 2015, he included another molecule to the formulation's surface functionalization, a NGR peptide (Asn-Gly-Arg), reporting an even greater antitumoral efficacy in comparison to all earlier formulations, in both the previously studied cell line and a new human breast adenocarcinoma one [90]. The other two reports were developed for pulmonary delivery. Kaur et al underwent a Box-Behnken design optimization of all conceivable parameters and evaluated the optimal formulation against a plain drug solution, reporting a circa 3-fold increase in paclitaxel lung concentration [91]. Lastly, Taratula et al developed a NLC co-delivery system containing paclitaxel (or doxorubicin) and siRNA for the suppression of proteins responsible for drug resistance in cancers, with the addition of a synthetic hormone analog as a targeting moiety specific to lung cancer cells. His data evidenced a much higher effectiveness with the targeted paclitaxel-NLC than with placebo and free paclitaxel with an almost complete cancer regression when siRNA is co-encapsulated [92].

Hence, it is obvious the utmost importance to explore deeper into the vastly untapped potential of paclitaxel-loaded nanostructured lipid carriers.

## NLC synthesis

To date, various techniques have been reported for the synthesis of lipid nanoparticles.

One of such is high pressure homogenization, which can be further divided into hot [93] and cold [94] variants. In both, the active compound is dissolved in the previously melted lipid blend. The variants then differ in the addition of a hot or cold aqueous surfactant solution, respectively, and the temperature at which the microemulsifying step is conducted. These techniques offer some advantages, such as a narrow particle size distribution with a low content of microparticles, avoidance of organic solvents and a great ease of scale-up accompanied by a frequent availability of the equipment required in industrial laboratories [95].

Another methodology is o/w microemulsion, which is based on the dispersion of warm microemulsions in cold water under stirring, leading to a nanoprecipitate [96]. Unfortunately, in this method a high concentration of surfactants and co-surfactants are used and results in very small yields. Variations of the previous method, also based on the breaking of an o/w microemulsion into a nanoemulsion, rely on solvent evaporation, diffusion or injection molding. In the emulsification-evaporation process, the lipid is first dissolved in an organic solvent and a microemulsion is created through the addition of an aqueous phase containing a surfactant. Subsequently, the solvent is left to evaporate under normal or reduced pressure while at room temperature, resulting in a nanoprecipitate in the aqueous medium, with the benefit of avoiding possible heating-related issues [97]. The emulsification-diffusion methodology, on the other hand, was developed for lipids which could not be dissolved in the organic solvent under

ambient conditions. Consequently, both the lipids and the solvent are mixed while in a heated water bath for the dissolution to occur. An addition of water to the organic solution results in coacervation and formation of lipid nanoparticles, which are then collected by ultracentrifugation, solvent evaporation or cross-flow filtration [98]. The third method, injection molding, represents a faster, mechanically-aided solvent-diffusion technique, as lipids dissolved in a water miscible organic solvent are rapidly injected into an aqueous phase, resulting in coacervation and a nanoparticle dispersion. This process has the specific advantage of a simultaneous efficiency, tight conditional control (by parameter variation) and simple mechanical implementation (the most technically complex apparatus is a syringe) [99]. However, all 3 of these methods sin on the utilization of organic solvents and their accompanying toxicological and environmental hazards. Additionally, the first two present a fairly dilute nanoparticle suspension, largely due to the limited solubility of lipids in the solvents.

A clever way to ensure a higher hydrophilic drug encapsulation efficiency resulted from the double emulsion technique. This method stands on the drug's dissolution and entrapment in the internal aqueous phase of a w/o/w emulsion, along with a stabilizer, in order to prevent its partitioning to the outer phases during solvent evaporation. It is initiated as a warm w/o microemulsion, resulting from the addition of drug, water, stabilizer and melted lipids, which is then dispersed into another stabilizer-containing water solution forming a w/o/w [100]. The nanoparticles are ultimately collected through diafiltration. This technique yields good results with sensitive drugs, such as peptides and nucleic acids, if an organic solvent is utilized for the lipid's dissolution instead of heat, although with the advent of common organic solvent disadvantages [101]. Another disadvantage is the relatively small aqueous inner compartment compared to the whole lipid matrix, resulting in, likewise, comparatively inferior encapsulation efficiencies.

NLCs can also be synthesized by ultrasonication in conjunction with [102], or absence of [103, 104], high shear homogenization. In this technique, lipids, surfactant and drug are all mixed together in a water bath at a high enough temperature to melt the lipids. Water, at the same temperature, is then added to the previous mixture, resulting in an emulsion, which is, optionally, subjected to high shear forces through high speed stirring, such as with a rotor-stator homogenizer, to form a microemulsion. Lastly, the particles undergo high strain during ultrasonication, due to cavitations caused by sonic waves, extremely elevated and localized temperature and pressure occurrences by collapsing bubbles, resulting in a suspension of nanoparticles. The greatest advantages of this methodology are the complete absence of organic solvents, ease and velocity of process and commonly available equipment. However, there is a possible metal contamination from particles released by the sonicator's tip, commonly associated with its usage, being it recently acquired or age-old. The other, much more frequent disadvantage is the broad particle size distribution, largely resolved by a higher surfactant concentration (which could, in turn, lead to toxicity issues) or the absence of high speed stirring. Additionally, it is possible to employ this technique in a standalone high sheer homogenization version [105], although unadvisable due to the stated broad distribution problem.

The standalone ultrasonication method, was the chosen technique for this work, due to the extensive experience in its employment, good advantage to disadvantage ratio and the presence of a sonicator in the laboratory.

*Reagents and equipment*

The chosen lipid blend comprise Gelucire® 43/01, Compritol® 888 ATO and Miglyol® 812 while the chosen surfactant Tween® 80.

Gelucires are blends of mono-, di- and triglycerides with polyethylene glycol esters of fatty acids marketed by Gattefossé. In particular, Gelucire® 43/01 has a melting point of 43°C and HLB of 1. Compritol® 888 ATO, also marketed by Gattefossé, is a blend of different esters of behenic acid with glycerol. It has a melting point of 70°C and HLB of 1. On the other hand, Miglyol® 812 is marketed by Acofarma Distribuición and comprised of a mixture of caprylic and capric triglycerides. It has a melting point lower than 0°C and HLB of 15.36. Tween® 80, the surfactant, is the trademark name for Polyethylene glycol sorbitan monooleate marketed under Sigma-Aldrich, a biocompatible and amphoteric molecule.

The described lipid combination was chosen taking into account the need of having a formulation which melted when the temperature arose higher than 40-45°C. Additionally, paclitaxel's solubility was taken into account by conducting lipophilicity tests. Compritol® 888 ATO was also added to counterbalance the melting point of Miglyol® 812 and to introduce an even higher degree of disorder to the nanoparticle's matrix, thereby increasing the drug load.

Paclitaxel was bought from LC Laboratories and utilized without further treatment.

The probe-sonicator utilized was a VCX130 from Sonics & Materials, Inc. (130 W of maximum potency) and the double-deionized water was filtered through a nanopore membrane (conductivity lesser than 0.1 $\mu S.cm^{-1}$).

*Ultrasonication technique*

The methodology herein described was an adaptation of the protocols followed by the research group and is summarized in **Figure 4**.

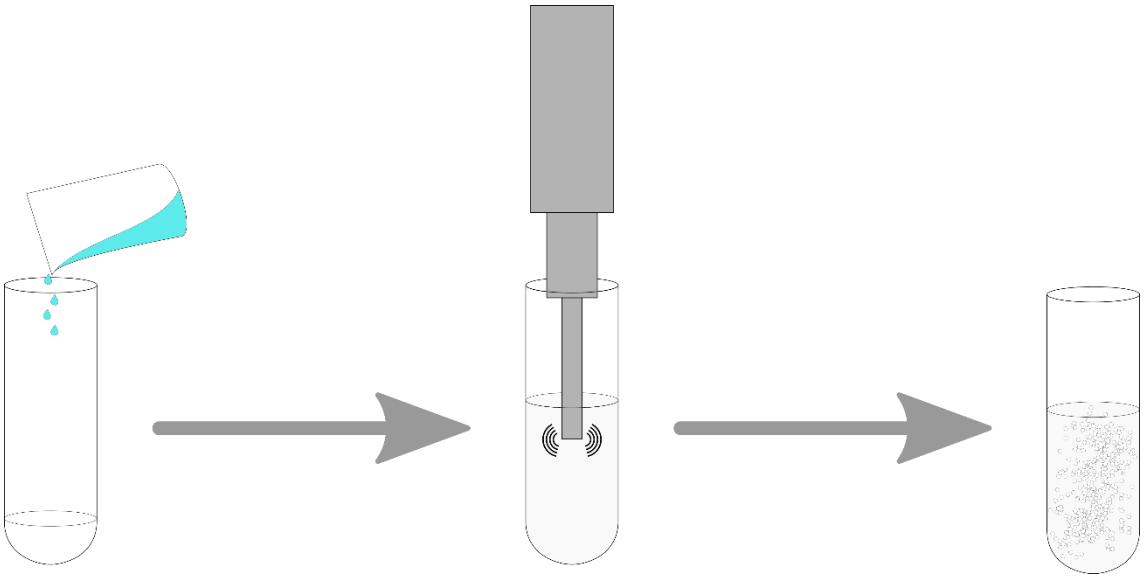

***Figure 4.*** *Representative diagram of the NLC synthesis process by a standalone ultrasonication technique. From left to right: addition of water to melted lipid, surfactant and drug, sonication and final product.*

The optimized formulation was synthesized as followed. 70% (w/w) of Gelucire® 43/01, 6% (w/w) of Compritol® 888 ATO, 10% (w/w) of Miglyol® 812, 12% (w/w) of Tween® 80 and 2% (w/w) of Paclitaxel were weighted and stored in a glass tube. The tube was then placed in a water bath at 75°C until all lipids had melted and magnetically stirred to suspend the drug. Afterwards, 16 mL of double distilled water, pre-heated at 75°C were added, obtaining an opaque, white suspension, which was placed under the probe-sonicator at 104 W of potency during 10 minutes. The resulting white nanoemulsion was stored in a sealed glass vial and left to cool at room temperature.

## Encapsulation efficiency assessment

Encapsulation, or entrapment, efficiency is defined as the percentage of encapsulated drug relative to the total added amount [106]. Hence, in this work, the percentage was determined by measuring the unentrapped paclitaxel's amount and calculating its inverse relativized to the absolute quantity initially added, as per the equation:

$$\%EE = \frac{Total\ amount\ of\ paclitaxel - Measured\ free\ paclitaxel}{Total\ amount\ of\ paclitaxel} * 100 \quad (2.1)$$

The study of the *in vitro* behavior of Paclitaxel in an aqueous medium is a gargantuan task, due to the difficulty of maintaining a good sink condition derived from Paclitaxel's infinitesimal water solubility. In order to overcome such difficulty, a hydrotropic agent was used, sodium salicylate, which has already been reported to increase Paclitaxel's solubility by 100 times at 1 M concentration [107].

The sodium salicylate was purchased from Merck and utilized without further modification.

Initially, the assessment of particle stability in sodium salicylate had to be made. Therefore, size and ζ-potential measures and aggregates determination were conducted under different concentrations of the hydrotrope. The Paclitaxel-loaded NLCs presented as stable at concentrations as high as 0.5 M, upon which they started to deform and aggregate.

For the unentrapped paclitaxel assessment, a formulation sample was diluted in double deionized water with sodium salicylate at 0.5 M concentration, at a 1:100 ratio, and placed inside an Amicon® Ultra-4 Centrifugal Filter Device (Millipore). Centrifugation was then performed using a Jouan BR4i multifunction centrifuge (Thermo Electron) with a fixed 23°-angle rotor at 3500 rotations per minute for 30 minutes (**Figure 5**). Afterwards, the supernatant, which contained the unentrapped paclitaxel, was collected and the concentration was quantified through a V-660 spectrophotometer (Jasco) at 200-400 nm.

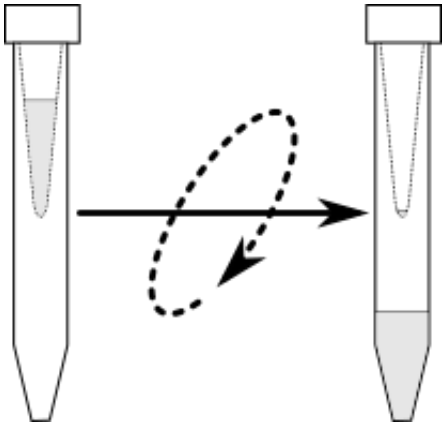

***Figure 5.*** *Centrifugation step of the encapsulation efficiency assessment methodology.*

## Characterization techniques

*Cryo-scanning electron microscopy (Cryo-SEM)*

The SEM technique relies on the emission of an electron beam from a tungsten filament, which, when it contacts with a sample's surface, provokes the ejection of low-energy secondary electrons by inelastic scattering, high-energy backscattered electrons by elastic scattering and x-ray radiation. These signals can be measured by different detectors to gather information about the topology and chemical composition of the sample [108].

SEMs operate under high vacuum, which tends to cause the nanoparticle's deformation, or even rupture, since NLCs are known to be very labile. Additionally, the ones synthesized during this work have a melting point of little higher than 40°C, increasing their fluidity to even higher proportions. To circumvent such limitations, a cryogenic variant of sample preparation was utilized, where the sample is previously fixed with liquid nitrogen.

The images obtained for this work were measured by a FEI Quanta 400FEG SEM system and conducted in *Centro de Materiais da Universidade do Porto* (CEMUP).

*Dynamic and Electrophoretic Light Scattering (DLS and ELS)*

When a light source emits radiation upon small particles, the light scatters, a phenomena known as Rayleigh scattering. If the source is a laser (monochromatic and coherent) the scattering suffers an intensity fluctuation due to the particles' Brownian motion. The information acquired, post autocorrelation, from this fluctuation permits the calculation of a particle's translational diffusion coefficient, which can be equated into the particle's hydrodynamic radius by the Stokes-Einstein-Sutherland equation:

$$r_h = \frac{k_B T}{6\pi\eta D} \tag{2.2}$$

where $r_h$ is the hydrodynamic radius, $k_b$ the Boltzmann's constant, T the absolute temperature, η the solution's viscosity and D the diffusion coefficient [109]. The hydrodynamic radius of a particle represents the radius of a hard sphere that diffuses at the same rate as the particle, which can be considered the same when applied to nanostructured lipid carriers since they are quasi-spheres.

Electrophoretic light scattering is a variant of the dynamic technique, where, instead of Brownian motion, an oscillating electric field is responsible for the particles' mobility. Through the data obtained, the particles' electrophoretic mobility is determined, which can then be related to their ζ-potential by a variety of models, the most common being Smoluchowski's:

$$v_E = 4\pi\varepsilon_0\varepsilon_r \frac{\zeta}{6\pi\eta}(1 + kr) \quad (2.3)$$

where $v_E$ represents the electrophoretic mobility, $\varepsilon_r$ and $\varepsilon_0$the relative dielectric constant and electrical permittivity of vacuum respectively, r the particles' radius and k the Debye-Hückel parameter [110]. The ζ-potential represents the nanoparticle's electric potential at the slipping plane, the boundary beyond which ions in solution do not suffer any interaction by the particle's mobility. This potential is closely related with the particle's stability in suspension.

For the purpose of this work, both size and ζ-potential measures were performed with a NanoBrook 90Plus PALS Particle Size Analyzer from Brookhaven Instruments Corporation, with the addition of a BI-ZEL electrode for ELS.

## Results and discussion

The synthesis methodology described above corresponds to the optimized NLC formulation, in respect to size, ζ-potential, polydispersity index and encapsulation efficiency. This optimization was conducted following an iterative approach, which is based on a *create-assess-learn-recreate* routine, applying changes in lipid ratios, water and surfactant content and sonication time and potency as needed.

In **Table 3** are depicted the physicochemical characteristics of a small fraction of the synthesized formulations. This table was kept summarized due to the sheer amount of NLCs synthesized.

***Table 3.*** *Physicochemical parameters of some of the synthesized NLC formulations during the optimization process.*

| ***Formulation #*** | **Size (nm)** | **Polydispersity index (adimensional)** | **ζ-potential (mV)** |
|---|---|---|---|
| *8* | 369.8 | 0.187 | -31.52 |
| *11* | 281.3 | 0.137 | -29.62 |
| *14* | 498.2 | 0.302 | -28.81 |
| *16* | 248.5 | 0.147 | - |
| *20* | 308.4 | 0.249 | - |
| *23* | 295.1 | 0.263 | - |
| *27* | 474.8 | 0.240 | -30.15 |
| *29* | 290.5 | 114.9 | - |
| *32* | 347.4 | 0.164 | - |
| *35* | 368.3 | 0.145 | - |
| *37* | 229.1 | 0.109 | - |
| *38* | 210.9 | 0.160 | - |
| *39* | 235.0 | 0.155 | - |
| *40* | 239.2 | 0.173 | - |
| *41* | 245.5 | 0.113 | -29.23 |

The ζ-potential started as being measured at every new formulation. However, when noticing it would only change within the electrode's sensibility range, it started to be measured at more spacious intervals. In a similar note, the relationship between encapsulation efficiency and the synthesis's parameters was not thoroughly examined, as this section was only meant to be used as a starting point in size, polydispersity and ζ-potential for the later experimental work and it was expected for it to drastically diverge when the magnetic nanoparticles were introduced, and therefore only on the last formulation was it assessed.

The optimized formulation presented a mean hydrodynamic diameter of 245.5 ±0.1 nm, with 99.96% of all nanoparticles below 117.83 nm, and polydispersity index of 0.113 ±0.008, both measured by DLS. Besides being greatly monodisperse, these results are in agreement with the initial objective of having a nanoparticle smaller than 200 nm to avoid capture by the Mononuclear Phagocyte System [111] and to take advantage of the Enhanced Permeation and Retention effect (EPR) [77]. The ζ-potential of -29.2 ±0.5 mV, measured by ELS, is considered optimal, since it leads to a lack of aggregation and low cytotoxicity [112]. The entrapment efficiency of the optimized formulation was found to be above 99%. It was not possible to ascertain a specific percentage due to the supernatant's absorbance being lower than the spectrophotometer's sensitivity. This result is slightly higher than the efficiencies reported by other authors, which ranged from 90% to 95% [56, 89-91].

Cryo-SEM imaging was utilized instead of the conventional TEM and SEM. Since the nanoparticles were engineered with the purpose of melting at around 40$^{o}$C, they have a high fluidity at room temperature. Due to this plasticity, the vacuum required for TEM/SEM imaging distorted the nanoparticles, leading to the necessity of freezing them prior to observations. The images collected (**Figure 6**) were in agreement with the results obtained by the light scattering techniques. Additionally, no noticeable change in diameter resulted from Paclitaxel's encapsulation.

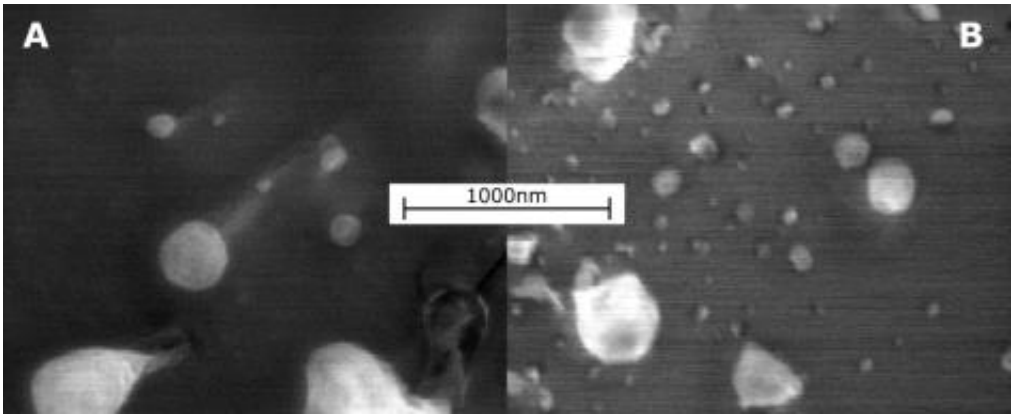


***Figure 6.*** *Cryo-SEM images of the placebo (A) and Paclitaxel-loaded (B) nanostructured lipid carrier formulation.*

# Chapter 3

## Magnetic nanoparticles

### Introduction

Magnetism occurs from the motion of electrically charged particles, such as protons, electrons and neutrons (although neutrons are neutral, they consist of smaller electrically charged particles) [113]. Hence, since every material in nature is composed by them, all have an intrinsic property called magnetization, **M**, which is regarded as the vector sum of all its individual constituents' magnetic moments. When a material is placed in contact with an external magnetic field, **H**, its magnetization creates a larger induced magnetic field, **B**, in a phenomena called magnetic induction, where $\mu_0$ represents the permeability of free space [114, 115]:

$$\boldsymbol{B} = \mu_0(\boldsymbol{M} + \boldsymbol{H}) \tag{3.1}$$

Since the magnetic properties of a material should be measured as a direct magnetization response dependent on an applied magnetic field, the magnetic materials categorization relies on the ratio between those two physical entities, which is called the magnetic susceptibility, **χ** [114, 115]:

$$\boldsymbol{\chi} = \mathbf{M}/\mathbf{H}, -1 < \chi < +\infty \tag{3.2}$$

There are two categories under which magnetic materials can be classified depending on their magnetic susceptibility: paramagnetism, when it is positive, and diamagnetism, when it is negative. Diamagnetism refers to the case where the magnetization in a material physically opposes the applied field H, consequently reducing it. Lenz's law states that "If an induced current flows, its direction is always such that it will oppose the change which produced it". Such statement means that, under an applied magnetic field, the electrons in atomic orbitals will slightly adjust their orbits with the intent of creating current loops that oppose said field [116]. The result is that every material has an innate diamagnetic property, albeit very small in most cases [117]. Nonetheless, even though all materials present diamagnetic properties, in some it is negligible compared to a positive magnetic susceptibility created by the magnetic moments of unpaired electrons when they align with an applied field, a property known as paramagnetism [118].

A less broad classification method relies on the relative ordering of the magnetic moments contained in a material (**Figure 7**). The absence of diamagnetic properties is due to the inexistence of magnetic moments in such substances. In paramagnetic materials, each magnetic moment is randomly oriented due to thermal energy, as shown in **Figure 7.A**. However, if the temperature decreases, the magnetic interaction between the magnetic moments predominates over the thermal energy's influence, causing a characteristic ordered state. In ferromagnetic materials (**Figure 7.B**), this ordering is parallel and happens below the Curie-Weiss temperature, while for antiferromagnetic materials (**Figure 7.C**) the ordering is antiparallel and occurs below the Néel temperature. These critical transition temperatures are

properties individual to each material's chemistry and magnetic characteristics. Lastly, there is a variant of antiferromagnetism where each interacting pair of magnetic moments have different magnitudes (**Figure 7.D**) [114, 115, 117, 118].

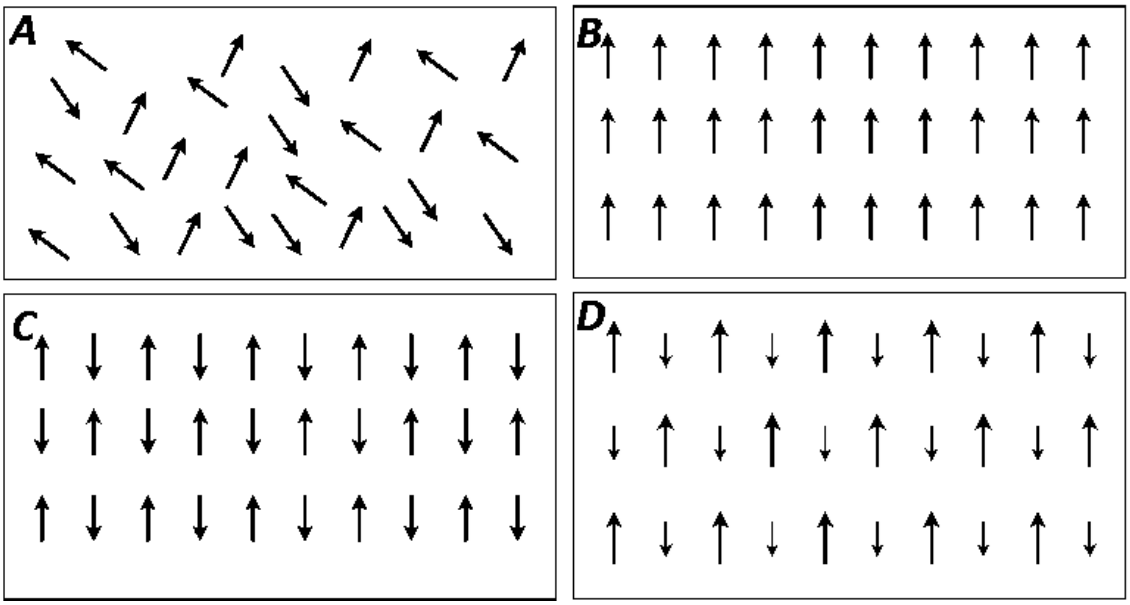


***Figure 7.*** *Possible orderings of magnetic moments: (A) paramagnetic; (B) ferromagnetic; (C) antiferromagnetic; and (D) ferrimagnetic states.*

There is one other magnetic state which these classifications fail to encompass, since it cannot be described by an ordering of domains. When a magnetic material is very small, ranging from atomic scale to a couple dozens of nanometers depending on the material (as example, circa 20 nanometers for magnetite [119]), it starts behaving as a single giant magnetic domain. In this state, materials behave similarly to paramagnets, by avoiding any reminiscent magnetization after the magnetic field removal, but have a much higher susceptibility [120]. Like the previously described magnetic states, superparamagnetic materials also have a critical transition temperature specific to each material's composition. However, since they are a single magnetic domain particle, below this temperature they are in a blocked state, ignoring any external field, hence it is known as blocking temperature [121].

The easiest way to distinguish between the different magnetic states is to analyze a material's M-H curve (**Figure 8**). If we apply an increasing magnetic field on a ferromagnet and subsequently decrease it, the magnetization does not follow the initial magnetization curve. This irreversibility is called hysteresis, and it occurs because the magnetic susceptibility is not a scalar, but a vector. At high applied fields, the magnetization approaches saturation magnetization, ($M_{sat}$), where every magnetic domain is aligned, and, when such field is removed, remanent magnetization ($M_r$), where some of the domains do not return to the original state. The sole manner to return these domains to their basal state is to apply a negative field, having a specific magnitude denominated coercive field ($H_c$) where the magnetization returns to zero. The hysteresis curve follows a symmetric pattern if the applied field varies from positive to negative values. Materials with a coercive field greater than 1000 $A.m^{-1}$ (circa 12 Oe) are called hard magnets, whereas soft magnetic materials are those with below that value [122]. In biological

applications, namely hyperthermia, high values of $M_s$ and, more importantly, low values of $H_c$ are required, as will be the case of superparamagnetism, where the coercivity is null.

Hyperthermia is a type of cancer treatment in which localized body tissue is exposed to high temperatures. At temperatures higher than 40°C the natural enzymatic processes that keep cells alive start to wane, rendering them more susceptible to the effect of radiation or chemotherapy while inducing apoptosis. At even higher temperatures (circa 45°C) human cells stop working all-together and die (necrosis) in a process known as thermoablation [123].

Magnetic nanoparticles have the ability to dissipate heat when subjected to an alternating magnetic field via magnetic losses, which can be distinguished into three different mechanisms – hysteresis, Néel and Brown relaxations. There are also other mechanisms: the magnetic loss by friction in viscous suspension and Foucault currents in metallic materials. However, both shall be omitted since they mainly affect larger particles.

Hysteresis losses (**Figure 9.C**) are a result of the uneven magnetization of the material during sequential magnetization cycles and may be derived from the integration of the hysteresis loops, representing the energy dissipated per cycle. They are the predominant loss mechanism in ferrimagnetic nanoparticles [124] and are inexistent in superparamagnetic materials, due to the obvious absence of hysteresis loops.

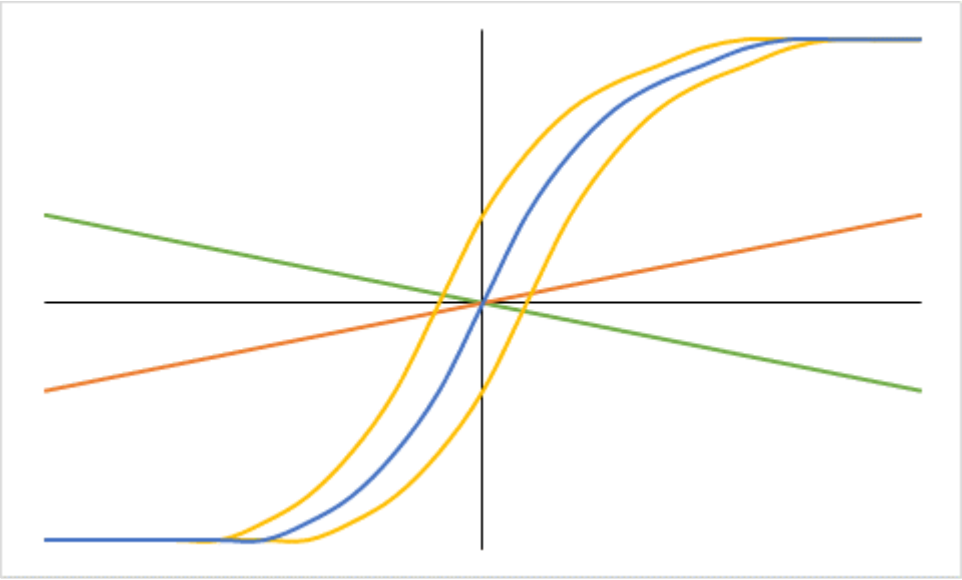

***Figure 8.*** *Illustrative magnetic field dependencies of different materials' magnetization during several magnetization cycles. Diamagnetism in green, paramagnetism in orange, superparamagnetism in blue and ferromagnetism, with its characteristic hysteresis loop, in yellow.*

In smaller nanoparticles, the heat dissipation is mainly caused by a delay in the relaxation of the magnetic moment. This moment behaves according to a uniaxial anisotropy, which means it only has two stable antiparallel orientations, both separated by an energy barrier. Therefore, two mechanisms are possible: either the magnetic moment manages to surpass the anisotropy barrier and shift while the particle remains fixed (**Figure 9.A**) or it fails and the particle rotates to compensate (**Figure 9.B**), causing energy dissipation by friction. Evidence shows that the first, Néel relaxation, holds a higher influence on superparamagnetic

nanoparticles [125, 126], while the second, Brown relaxation, is heavily influenced by the surrounding fluid's viscosity [124]. Additionally, the heating rate is very dependent on particle size, while being maximized by a low polydispersity [126, 127].

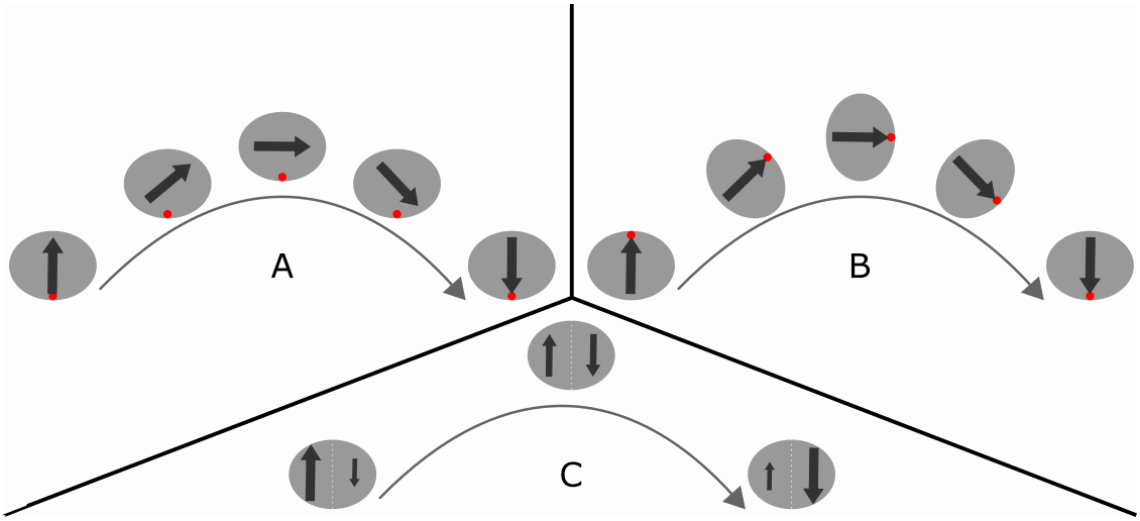


***Figure 9.*** *Illustrative representation of the three heat generating mechanisms by magnetic losses: Néel relaxation (A); Brown relaxation (B); and hysteresis (C).*

Besides having a higher heating efficiency in comparison to larger multi-domain magnetic materials [128], superparamagnetic nanoparticles have many characteristics that make them ideal for a therapeutic approach. With the lack of a hysteresis loop, superparamagnetic materials do not retain magnetization once the external magnetic field is removed, thus avoiding particle agglomeration and complications thereof [129]. Despite extensive cell viability assays performed in regards to the cytotoxicity of superparamagnetic iron oxide nanoparticles (SPIONs), no considerable effect has been found at concentrations where other materials do exhibit it [130, 131].

## SPIONs synthesis

In past years, multiple synthetic approaches have been taken in order to obtain the perfect iron oxide nanoparticle. One of the earliest, and still much in use, was reported by Massart in 1981 [132], which he called co-precipitation. It consists in the addition of a base to an aqueous solution of ferrous ($Fe^{2+}$) and ferric ($Fe^{3+}$) ions in a 1:2 stoichiometric ratio under an oxygen free environment, preventing further oxidation, resulting in a black precipitate of less than 20 nanometers magnetite particles. Albeit this method offers an ease of controlling the nanoparticle's size by adjusting the pH, reaction temperature, stoichiometric ratio and iron precursors, such ease is severely limited [133]. Additionally, without further surface modification, the nanoparticles are prone to be oxidized into γ-$Fe_3O_4$ [134]. To circumvent these limitations, other methods were elaborated, such as microemulsion (water in oil) [135, 136], limiting the crystal growth to the inside of micelles, hydrothermal [137, 138] and solvothermal decomposition [139, 140], disassembling large iron-containing molecules in aqueous and organic solvents, respectively, and the sonochemical method [141, 142], utilizing acoustic cavitation to create extreme heat and pressure localized conditions. However, each of these methodologies is accompanied by their own disadvantages, such as a difficult scale-up or the use of highly toxic solutions. As if to keep up with technology advancements, some variants of

the previous methods were adapted to take advantage of microwaves [143-145]. This type of radiation allows for a much faster and uniform heating, which consequently leads to quick, reproducible and efficient reactions [146].

During this work, due to a lack of experimentation in the field, multiple methods and optimizations in regards to SPION synthesis had to be employed. Choices were focused on co-precipitation techniques, since these required no organic solvents and, theoretically, resulted in a large yield of smaller than 20 nanometers magnetic iron oxide nanoparticles.

The iron-based powders were attained through Sigma-Aldrich and the ammonium hydroxide 25% solution was purchased from Merck with no extra purification step conducted. All water utilized was double-deionized with a conductivity inferior to 0.1 $\mu S.cm^{-1}$.

*Conventional co-precipitation method*

The synthetic process utilized was based on the one described by Mahdavi et al, with some slight modifications [147].

In a typical procedure, ferric chloride hexahydrate ($FeCl_3 \cdot 6H_2O$) and ferrous chloride tetrahydrate ($FeCl_2 \cdot 4H_2O$), in a 2:1 molar ratio, were dissolved in 150 mL of double distilled water inside a three-necked closed flask, under a constant flow of nitrogen and vigorous magnetic stirring. After heating to 100°C, 20 mL of ammonium hydroxide (25%) was quickly added, turning the solution black. 30 minutes later, 3 mL of oleic acid was injected dropwise. The solution was then left stirring for one hour. Finally, the black precipitate was collected by magnetic separation with a strong permanent magnet and washed several times with double distilled water.

*Microwave-assisted co-precipitation method*

The microwave synthesis was carried out in a Discover® SP microwave system, automated by Explorer-12 software, using 25 mL glass vessels with Teflon caps, all purchased from CEM Corporation. The reaction temperature was controlled by built-in sensors, allowing the wattage to increase or decrease as needed, with a 300 W maximum. Pressure was also left unregulated, allowing the vessels to self-vent as needed, with a 200 psi maximum.

The optimized procedure was conducted as followed. $FeCl_2 \cdot 4H_2O$ and $FeCl_3 \cdot 6H_2O$ were dissolved in 20 mL of double distilled water in a vessel under vigorous magnetic stirring. The stoichiometric ratio used was 1:1.8 to account for the probable oxidation of $Fe^{2+}$ to $Fe^{3+}$ and the total iron concentration was chosen as 0.07 molar, due to it being inside the optimum range. 3 mL of 25% ammonium hydroxide was then rapidly added and the vessel removed from the stirring. After the precipitate settled, the vessel was placed inside the microwave system and the temperature set to 100°C, under maximum stirring, during 10 minutes. After the elapsed time, pressured nitrogen gas was injected into the system to quickly lower the temperature until 70°C to stop the reaction. Lastly, the black precipitate was collected with a strong permanent magnet, washed 2 times and suspended in 25 mL of double distilled water. The nanoparticles were then stored in a 50 mL Falcon® at room temperature.

## Characterization techniques

*Transmission Electron Microscopy – TEM*

TEM systems utilize a higher energy electron beam than SEM techniques, which, consequently, manages to interact with a sample at higher depths and achieve better resolution [148].

The SPION images were obtained from a JEM-1400Plus Transmission Electron Microscope in *Instituto de Biologia Molecular e Celular* (IBMC). Uranyl acetate (1%) was used as contrast agent.

*X-ray Powder Diffraction – XRD*

When x-ray waves are emitted into a crystalline solid they are absorbed by the atoms in the lattice, which then re-emit electromagnetic waves of the same frequency. The angle upon which the x-ray waves approach the atom plane will cause the emitted waves to undergo either a constructive or destructive interference, originating a maximum intensity when the wavelength is an integer multiple of the distance between two atoms.

A diffraction pattern can therefore be assembled by registering the emitted wave's intensity as a function of the incident angle. In it, the peaks' positions depend on the periodicity of the structure (i.e. the dimensions of the unit cell), whereas the peaks' relative intensities relate to the distribution of scattering matter (i.e. the atoms or molecules) within the unit cell, which, in the case of XRD, is the electron density. Such relations equate into a unique diffraction pattern for every material, which allows their identification by a comparison with known patterns stored in databases [149, 150].

The powder diffractometer utilized during this work was a Rikagu Smartlab (9KW) from the Institute of Material Physics of University of Porto.

*Superconducting Quantum Interference Device – SQUID*

SQUIDs are a type of extremely sensitive magnetometer which can measure magnetic fields as low as $10^{-14}$ T, due to a component called Josephson junction, an electronic circuit very sensitive to magnetic fluctuations. Since these circuits need to operate at near zero K temperatures, SQUIDs are equipped with a liquid helium refrigeration system [151].

For the purpose of this work, the magnetometer was utilized to measure the material's magnetic response as a function of the applied magnetic field to determine the magnetic saturation, coercivity and residual magnetization and as a function of temperature in both zero field cooled and field cooled techniques to ascertain the blocking temperature and degree of superparamagnetism.

All measures were taken in a Quantum Design superconducting quantum interface device (SQUID) from the Institute of Material Physics of University of Porto.

## Results and discussion

The initial particles, synthesized by the conventional co-precipitation method, were analyzed by DLS, which determined their size to be circa 1 micrometer. Since the objective of this work requires magnetic particles of smaller diameters, an exhaustive optimization process

was performed and, inclusively, the synthesis method was changed. All the nanoparticles were synthesized by the microwave-assisted method, which proved to be more reliable and extremely faster.

During the course of all the experimental process, all the synthesized nanoparticles remained stable in the solution, showing no signs of aggregation or precipitation.

As a somewhat crude method to evaluate the SPIONs' magnetic capabilities, a small permanent magnet was put into contact with the vial during a 5 second timeframe. This method was applied to all synthesized magnetic nanoparticles, as it represents a very quick, reliable and inexpensive procedure to ascertain a prognosis of the nanoparticle's magnetic character.

In **Figure 10** it is possible to denote the three different stages of such method during the referenced timeframe. Before the approach of the permanent magnet, the solution is a completely dispersed, opaque, black suspension. However, at the moment of magnetic exposure, the nanoparticles are met with a near-instant attraction, resulting in a progressive purification of the aqueous medium until, proceeding an elapsed time of circa 5 seconds, all the SPIONs concentrate, as close as they can to the permanent magnet, in a magnetic slurry. Afterwards, a simple vigorous agitation returns the solution to its prime condition.

***Figure 10.*** *SPION solution response to a small permanent magnet. From left to right: the baseline suspension state prior to magnetic exposure; 1 second after the magnet's placement; and 5 seconds of magnetic influence.*

The magnetic nanoparticles' morphological analysis was executed by TEM imaging, which indicated sizes ranging from 5 to 15 nanometers and spherical shape (**Figure 11**).

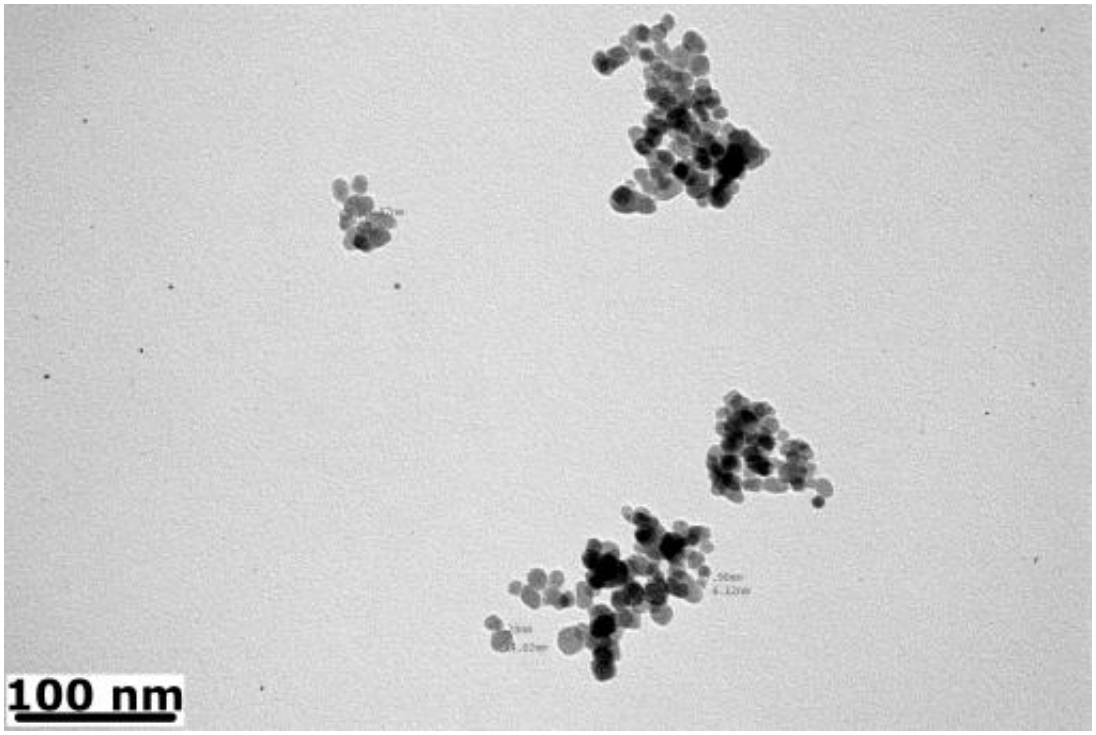


***Figure 11.*** *TEM image of microwave-assisted synthesized SPIONs with TEM-assisted size measurements.*

The structural characterization was made by XRD. **Figure 12** presents the diffraction pattern of the synthesized nanoparticles in comparison to that of pure magnetite, which was obtained from the RRUFF database (RRUFF ID: R061111.9). The peaks' juxtaposition indicates a high crystallinity of the SPIONs and the likely presence of a single magnetic phase. It is however possible the existence of a small amount of maghemite undiscernible by the XRD pattern, since its diffraction peaks differ from those of magnetite for only a few degrees leading to overlaps and consequent occlusions [152].

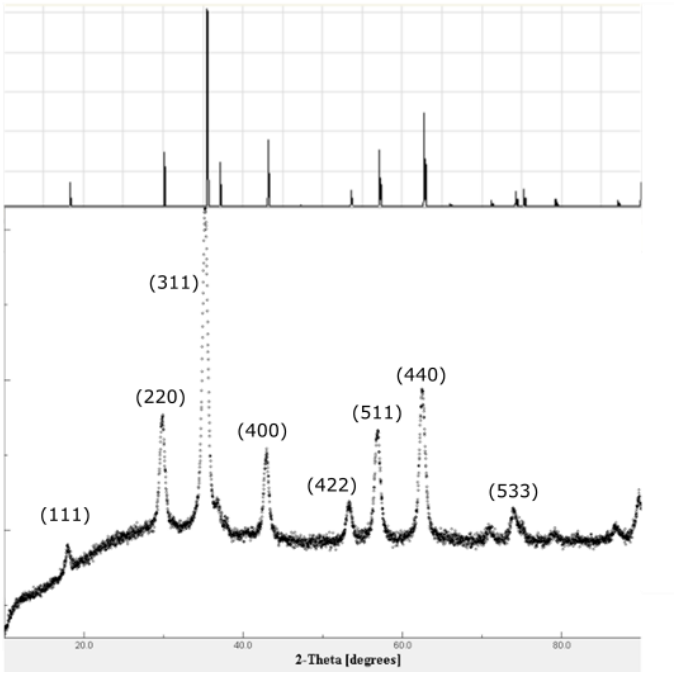


***Figure 12.*** *XRD diffraction patterns of pure magnetite (top) and the synthesized SPIONs (bottom).*

The nanoparticle's magnetic characterization was conducted through SQUID measurements. According to the magnetization measurements as a function of the applied magnetic field (**Figure 13**), the magnetite nanoparticles have a remarkable magnetic coercivity of 6 Oe at room temperature. However, with decreasing temperature the coercivity increases, reaching 180 Oe at 10 K. Since 10 K is sure to be below the blocking temperature, the increase of coercivity can be explained by the blocked state of the nanoparticles' magnetic domains, in which the fluctuation of magnetization is severely impaired and confers the "magnetic memory" commonly associated with ferromagnetic materials, which means the formulation contains a few multi-domain particles.

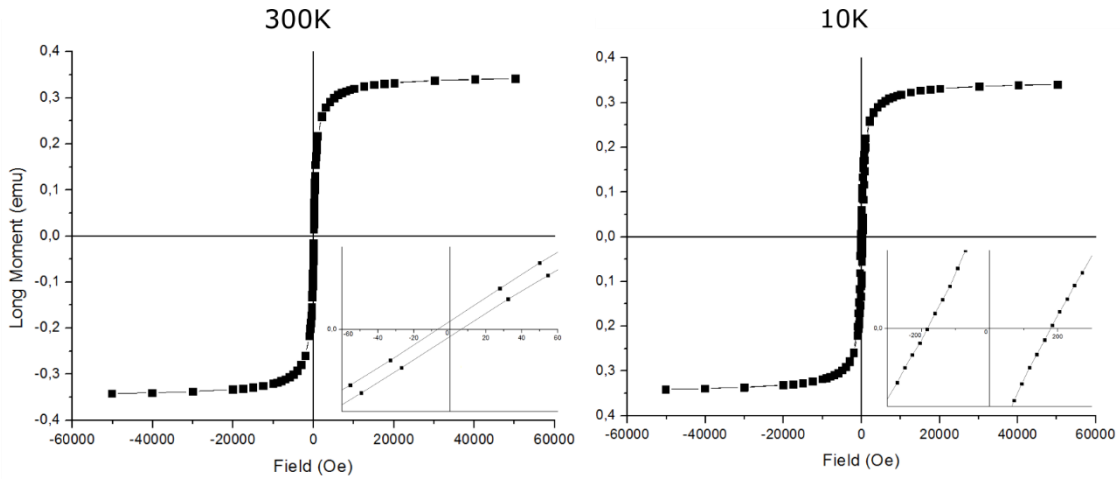


***Figure 13.*** *M(H) SQUID measurements of the synthesized SPIONs, at 300K and 10K, and a centered, zoomed version of each.*

To gather further information on the SPIONs blocking temperature, zero-field-cooled (ZFC) and field- cooled (FC) measurements were conducted (**Figure 14**).

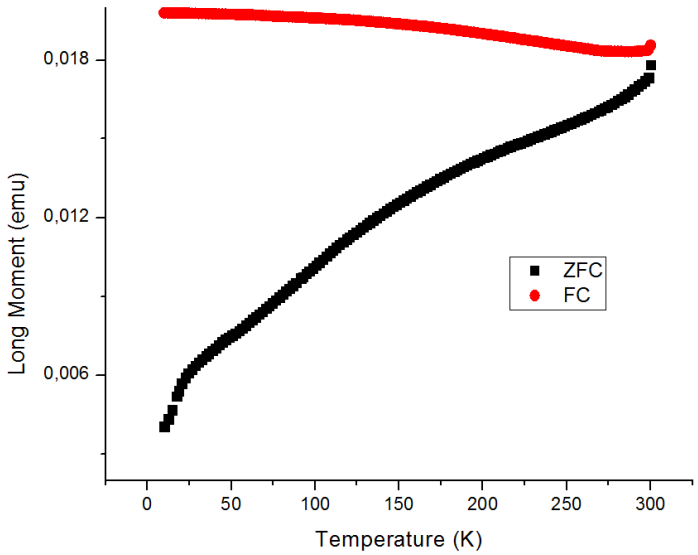


***Figure 14.*** *Zero-Field-Cooled and Field-Cooled measurements of the synthesized SPIONs.*

The SPION sample was first cooled to 5 K under no magnetic field and then slowly heated to 300 K under the effect of a 50 Oe field. Afterwards, still under the applied magnetic field, the sample suffered another temperature cycle. The magnetic measurements were all made during the heating phase. The FC curve presents a well-defined plateau, most likely unveiling the presence of strong dipolar interactions between the particles. These interactions also explain the ZFC curve's quasi-linear behavior, having no pronounced inflections, which precludes the determination of the blocking temperature, since the interactions cause it to shift to higher temperatures [153]. However, there is a slight change in the ZFC curve's increase rate at 25 and 150 K, which represents the unblocking of some of the smaller nanoparticles in the sample.

Therefore, the data acquired confirms the successful synthesis of somewhat polydisperse superparamagnetic iron oxide nanoparticles, with strong interparticle dipolar interactions.

# Chapter 4

## SPION-Paclitaxel-loaded Nanostructured Lipid Carriers

### Introduction

Aristotle once said: “The whole is greater than the sum of its parts”. Little did he know how this synergistic concept could be applied in nanotechnology.

As described in the previous chapters, superparamagnetic iron oxide nanoparticles have received much attention by the nanomedicine scientific community. Recently, an idea has surfaced to combine both the magnetic and lipid/polymeric nanoparticles to create a hybrid containing the advantages of both worlds.

Lipid-based and polymeric nanoparticles are extensively used as drug vehicles due to their ease of chemical and structural modulation to achieve a controlled *in vivo* circulation and release of drugs (improved bioavailability and half-life), and a tissue-selective targeting, which results in a minor biodistribution, in a reduced quantity of the active compound required and, therefore, in reduced possible side effects. Moreover, the nanoparticles act as a barrier to drug release, effectively controlling its solubility and diffusivity [154]. With the addition of magnetic nanoparticles to the formulation, these advantages widen to encompass hyperthermic capabilities. Additionally, due to this unique combination, the increase of heat can not only promote cell death but also the nanoparticle’s enhanced permeability or even total burst release by affecting its matrix’s fluidity (**Figure 15**). However, despite all of the promising advantages, this field has not received much attention.

Müller et al demonstrated, in 1996, the possibilities arising from SPION encapsulated polymeric and solid lipid nanoparticles [155]. Since then, most of the focus was directed to magnetoliposomes [7, 156-158]. There have also been reports of successful encapsulation of magnetite particles in SLNs [159-161]. However, at the time of writing, the author was unable to locate reports of SPION-loaded nanostructured lipid carriers and their applications.

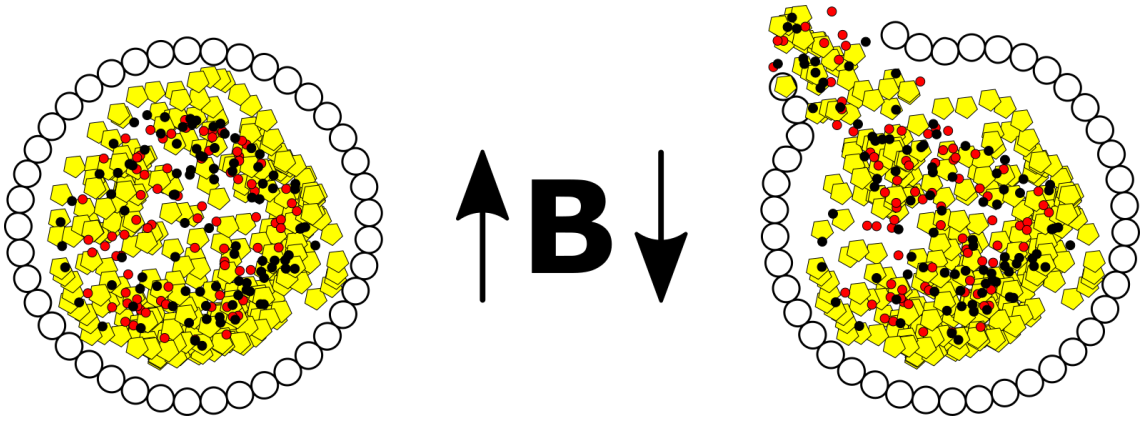


***Figure 15.*** *Illustrative representation of hyperthermia-aided release in a lipid nanoparticle.*

## SPION-loaded NLC synthesis

The synthesis protocol (**Figure 16**) followed was a slight adaptation of the one described in Chapter 2, taking into account the addition of magnetic nanoparticles.

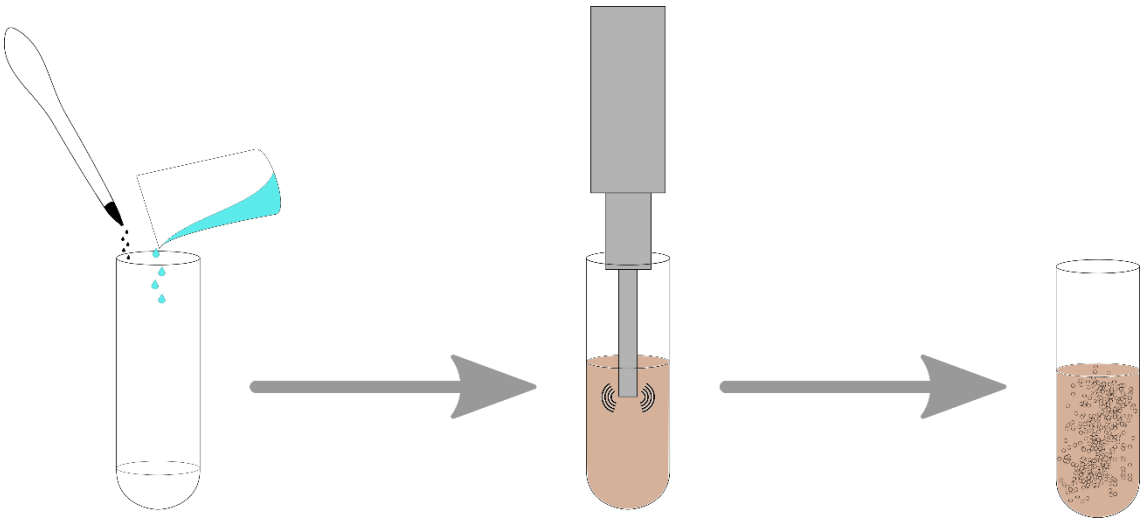

***Figure 16.*** *Representative diagram of the SPION-NLC synthesis process by an ultrasonication technique. From left to right: addition of water and SPIONS to melted lipid, surfactant and drug, sonication and final product.*

In a typical procedure, 70% (w/w) of Gelucire® 43/01, 6% (w/w) of Compritol® 888 ATO, 10% (w/w) of Miglyol® 812, 12% (w/w) of Tween® 80 and 2% (w/w) of Paclitaxel were weighted and placed in a glass tube. The tube was then submerged in a water bath at 75°C until all lipids had melted and magnetically stirred to suspend the drug. Afterwards, 16 mL of double distilled water, pre-heated at 75°C and 1 mL of room temperature SPION solution (as prepared by the method described in Chapter 3) were added, obtaining an opaque, brown suspension, which was placed under the probe-sonicator at 104 W of potency during 10 minutes. The resulting brown nanoemulsion was stored in a sealed glass vial and left to cool at room temperature.

## Box-Behnken experimental design

In statistics, Box-Behnken are a type of experimental designs for surface response methodology. Their prime usefulness lies on the clever positioning of the process space boundaries, leading to fewer design points and, therefore, less expensive and time consuming [162]. Numerous reports have confirmed the eligibility of this experimental design for nanopharmaceutics optimization [103, 163-166].

The Box-Behnken design utilized for the purpose of optimizing the SPION-, Paclitaxel-loaded NLCs was trifactorial (**Figure 17**) with three responses. The factors in use were the Gelucire® 43/01 to Miglyol® 812 ratio, amount of Paclitaxel and duration of sonication, while the responses measured were the nanoparticles' size, polydispersity and encapsulation efficiency. All factors consisted of a three level combination of high, low and midpoint.

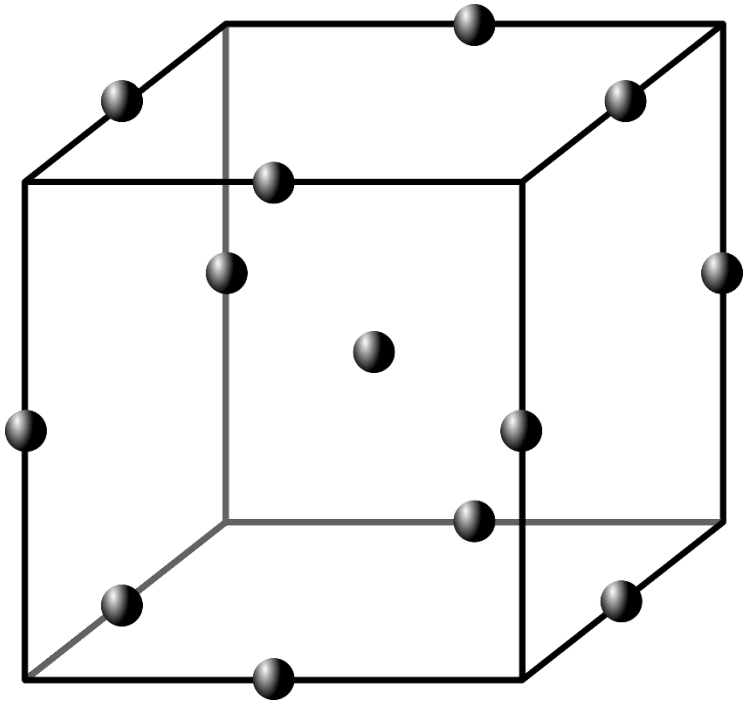

***Figure 17.*** *Design geometry for the Box-Behnken 3-factor design.*

## Release studies' methodology

One of the most important characteristics of a newly engineered drug-loaded nanoparticle is its release kinetics. Numerous methods have been reported to assess such kinetics, among which the most common were ultracentrifugation, centrifugal ultrafiltration and pressure ultrafiltration. Potential issues arising from these techniques include a deficient physical separation, causing the presence of nanoparticles in the measured sample and leading to significant measurement errors, particularly early in the release timescale [167]. Nowadays, the dynamic dialysis method is almost exclusively utilized for this kinetic assessment since it overcomes the previously described issues by avoiding the frequent separation processes [168].

The dialysis device utilized was a Float-a-Lyzer® G2, marketed by Spectrum Laboratories, with 1 mL of working volume and a molecular weight cutoff of 3.5 to 5 kDa.

For the release kinetics study, 1 mL of the synthesized NLC formulation was placed inside a previously moist dialysis tube. The surrounding medium was a Phosphate Buffer Solution containing sodium salicylate at 0.5 M concentration and pH-corrected with hydrochloric acid as needed. The assay was conducted at 37°C and at the pH levels of 7.4 and 6.3 to simulate physiological and neoplastic conditions, respectively. Samples were collected hourly during 8 hours for three consecutive days and analyzed with a spectrophotometer at 200-400 nm.

## Results and discussion

As previously described, a Box-Behnken design was elaborated for the purpose of nanoparticle optimization. This design implicated the synthesis of 15 different NLC formulations and their individual characterization. In **Table 4** are depicted the variables modified between these formulations and **Table 5** shows their physicochemical characterization. The nanoparticle's size utilized herein after is a weighted average of the biggest population (in

number) and not the mean diameter calculated by the software, since the NLC suspension contains a few large outlier nanoparticles which contribute to an erroneous computational analysis.

***Table 4.*** *Synthesis variables for the trifactorial Box-Behnken experimental design.*

| ***Formulation #*** | **Solid to liquid lipid ratio** | **Amount of loaded drug (mg)** | **Sonication time (min)** |
|---|---|---|---|
| *1* | 5 | 5 | 10 |
| *2* | 7 | 5 | 10 |
| *3* | 5 | 15 | 10 |
| *4* | 7 | 15 | 10 |
| *5* | 5 | 10 | 5 |
| *6* | 7 | 10 | 5 |
| *7* | 5 | 10 | 15 |
| *8* | 7 | 10 | 15 |
| *9* | 6 | 5 | 5 |
| *10* | 6 | 15 | 5 |
| *11* | 6 | 5 | 15 |
| *12* | 6 | 15 | 15 |
| *13* | 6 | 10 | 10 |
| *14* | 6 | 10 | 10 |
| *15* | 6 | 10 | 10 |

***Table 5.*** *Physicochemical characteristics of the synthesized NLCs.*

| ***Formulation #*** | **Nanoparticle size (nm)** | **Polydispersity Index (adimensional)** | **Encapsulation efficiency (%)** |
|---|---|---|---|
| *1* | 54.0 | 0.152 | 68.0 |
| *2* | 172.3 | 0.133 | 70.3 |
| *3* | 110.8 | 0.181 | 90.3 |
| *4* | 104.9 | 0.151 | 79.4 |
| *5* | 131.1 | 0.160 | 82.8 |
| *6* | 82.7 | 0.185 | 79.4 |
| *7* | 57.6 | 0.145 | 77.9 |
| *8* | 94.9 | 0.165 | 81.1 |
| *9* | 126.5 | 0.166 | 64.3 |
| *10* | 104.9 | 0.186 | 87.2 |
| *11* | 144.9 | 0.150 | 66.4 |
| *12* | 132.1 | 0.168 | 76.4 |
| *13* | 128.8 | 0.181 | 81.0 |
| *14* | 126.8 | 0.162 | 77.1 |
| *15* | 129.23 | 0.149 | 80.2 |

Box-Behnken design softwares illustrate the dependencies of measured responses to the factorial variables by tridimensional graphics. Three of the obtained graphics are depicted in **Figure 18**.

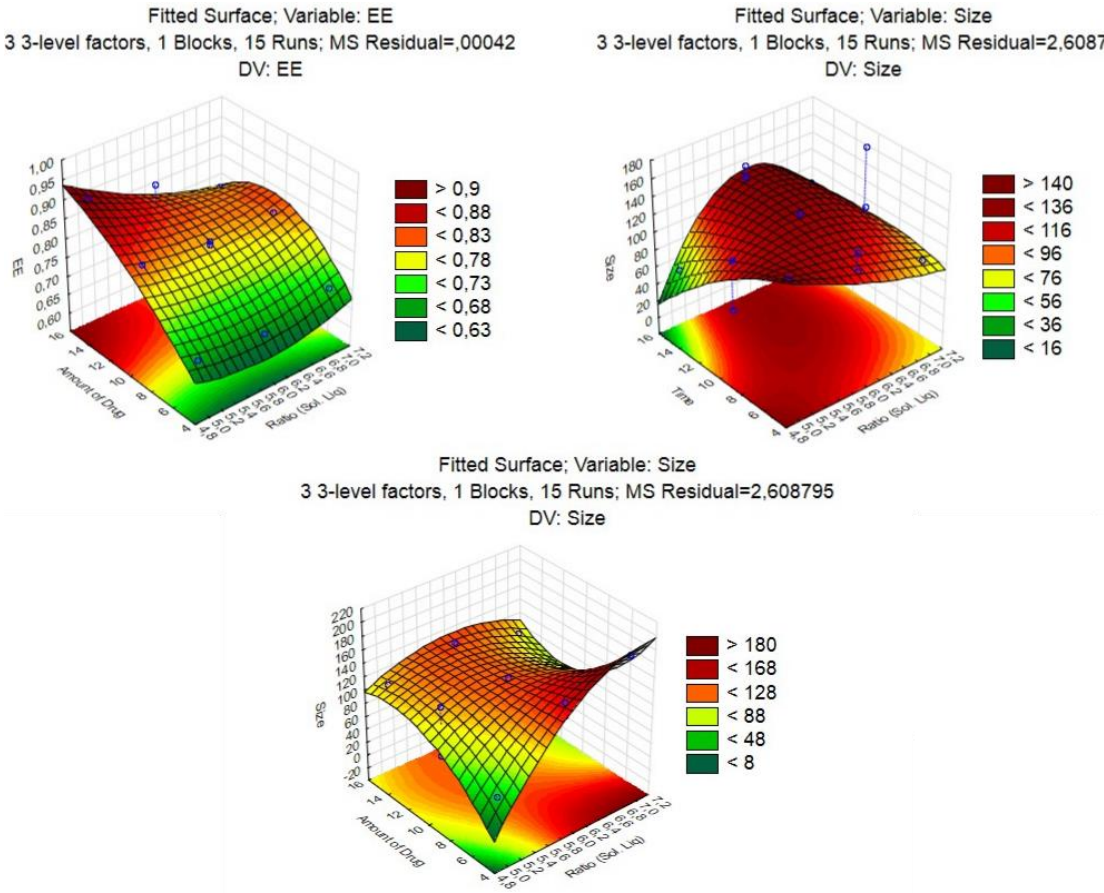


***Figure 18.*** *Graphical representation of three of the dependencies determined by the Box-Behnken design. Top left: Encapsulation efficiency according to amount of drug (y axis) and solid to liquid lipid ratio (x axis); Top right: Particle diameter according to time (y axis) and solid to liquid lipid ratio (x axis); Bottom: Particle diameter according to amount of drug (y axis) and solid to liquid lipid ratio (x axis).*

According to the calculations accomplished through the Box-Behnken software, all the synthesis parameters had a significant influence on the formulations' measured physicochemical characteristics.

The formulation chosen to conduct the remainder of this work was formulation 8, due to its acceptable compromise between polydispersity and encapsulation efficiency, while retaining the ideal size below 200 nanometers.

During the weeks encompassing the experimental procedures, the NLCs showed no signs of precipitation or degradation, indicating a positive stability. Additionally, the suspension's light brown color and lack of black precipitate was evidence of successful SPION encapsulation.

**Figure 19** depicts a simple visual comparison regarding the presence of magnetic nanoparticles in 5 weeks old formulations. First and foremost, the highly evident alteration is a change in the suspension's color from white (**Figure 19.B**), in SPIONs' absence, to a light brown (**Figure 19.A)**, in the complete formulation. Additionally, a very interesting aspect of the SPIONs' encapsulation is their ability to drive the NLCs upon a magnetic field exposure as evidenced by **Figure 19.C**.


***Figure 19.*** *Comparison between the NLC-Paclitaxel-loaded (A) and Paclitaxel-loaded formulations (B) and the magnetic field influence on the first (C).*

Cryo-SEM was used to further analyze the nanoparticle's morphology and evaluate their comparison to the previously synthesized simpler NLCs.

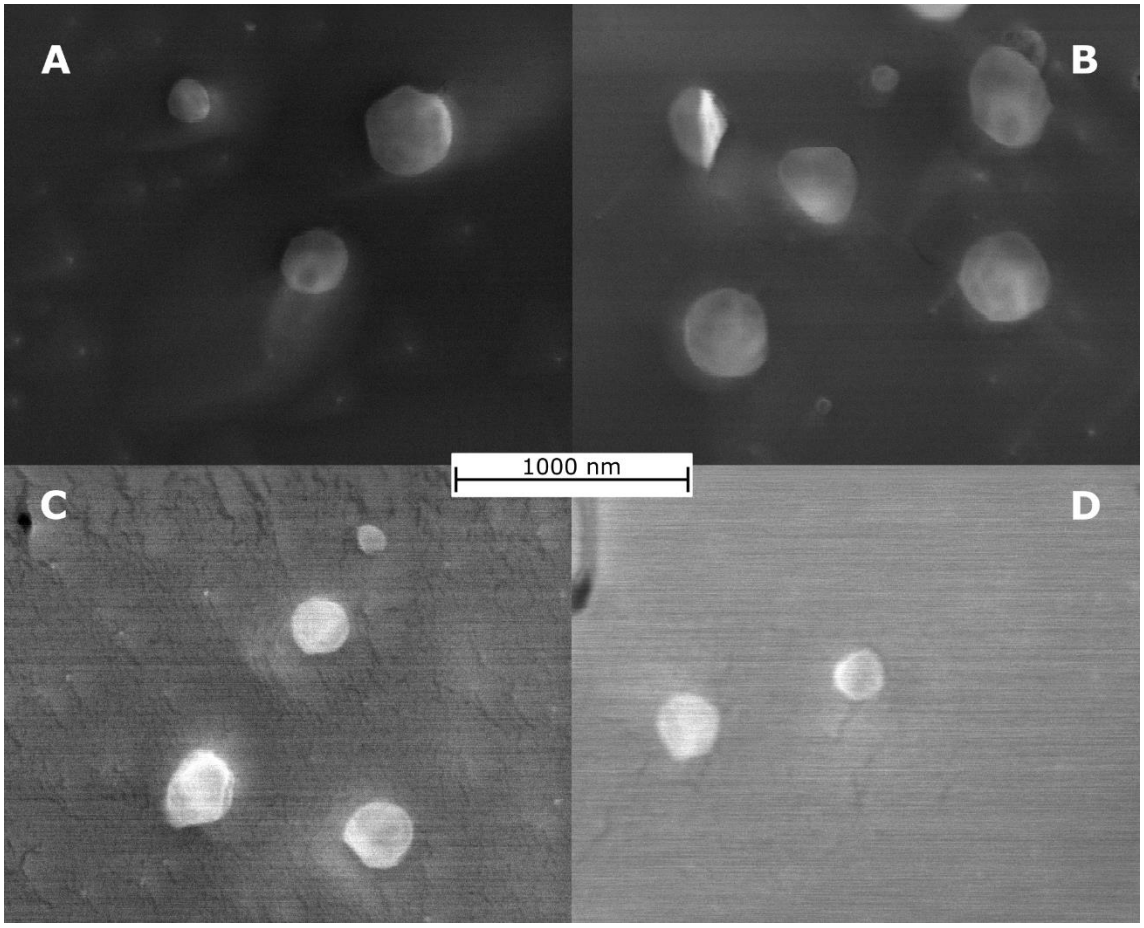


***Figure 20.*** *Cryo-SEM images of placebo NLCs (A), Paclitaxel-loaded NLCs (B), SPION-loaded NLCs (C) and SPION-Paclitaxel-loaded NLCs (D).*

Through the images provided by the electronic microscope it is possible to notice a decrease in diameter and polydispersity as a consequence of SPION encapsulation (**Figure 20.A** to **Figure 20.C**). Additionally, there is no noticeable change between placebo and drug encapsulating NLCs (**Figure 20.A** to **Figure 20.B** and **Figure 20.C** to **Figure 20.D**). As expected, all nanoparticles showed to be quite labile even while frozen.

To further ascertain SPION successful encapsulation, XRD was utilized and the resultant spectrum of the NLCs was compared to that of pure magnetite (**Figure 21**). All of the characteristic magnetite peaks are present, with the exception of the first at circa 18 degrees, which is absent due to a wide peak of, presumably, Gelucire® 43/01, indicating the presence of the SPIONs in the NLCs' interior.

The magnetic characterization proceeded similarly to the one described for free SPIONs. Additionally in a similar fashion, the coercivity had a value of 6 Oe at 300 K, indicating a superparamagnetic behavior, and 288 Oe at 10 K, due to the previously elucidated reason (**Figure 22**). However, at all temperatures, the magnetization suffered a steep decline after reaching saturation. The most likely explanation for such is based on the diamagnetic properties of the NLCs' lipidic matrix. With SPION-Paclitaxel-loaded NLCs, there are five magnetic states in balance exerting a force in the outer field: the SPION's superparamagnetism and diamagnetism, the Paclitaxel diamagnetism, the NLC's lipids' diamagnetism and the sample support's diamagnetism. At low applied fields, the superparamagnetism effect is prevalent over all the

other forces combined. However, after reaching saturation, its effect can no longer increase and the diamagnetic effects take hold. It is possible to correct the values by eliminating the influence of this diamagnetic effect (**Figure 23**).

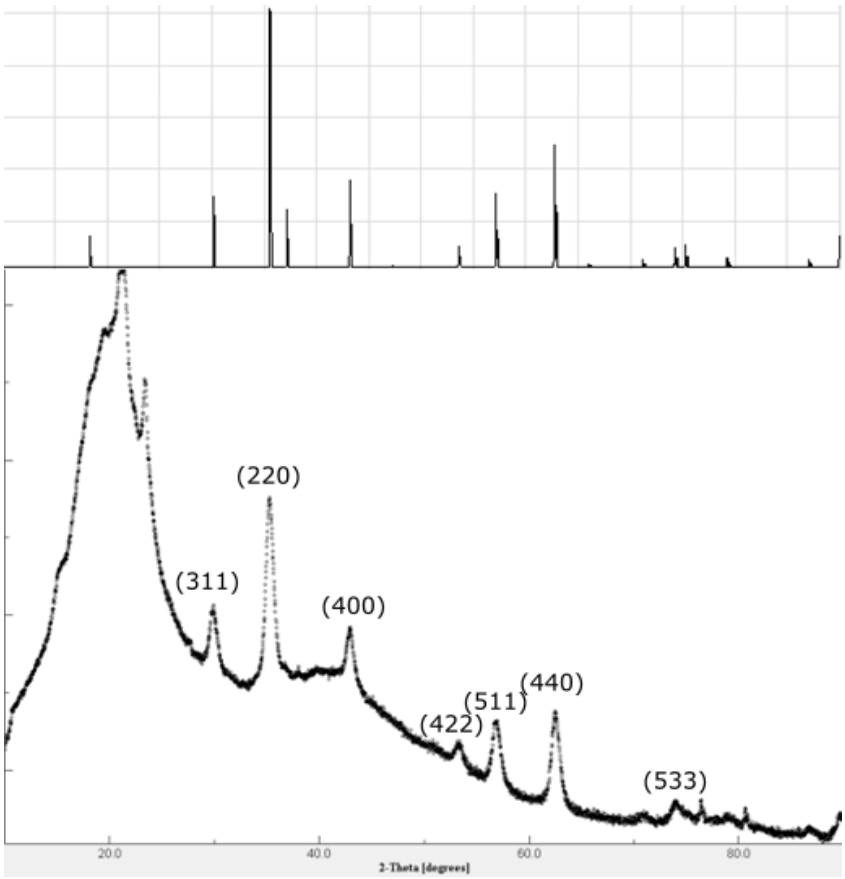


***Figure 21.*** *XRD diffraction patterns of pure magnetite (top) and the synthesized SPION-Paclitaxel-loaded NLCs (bottom).*

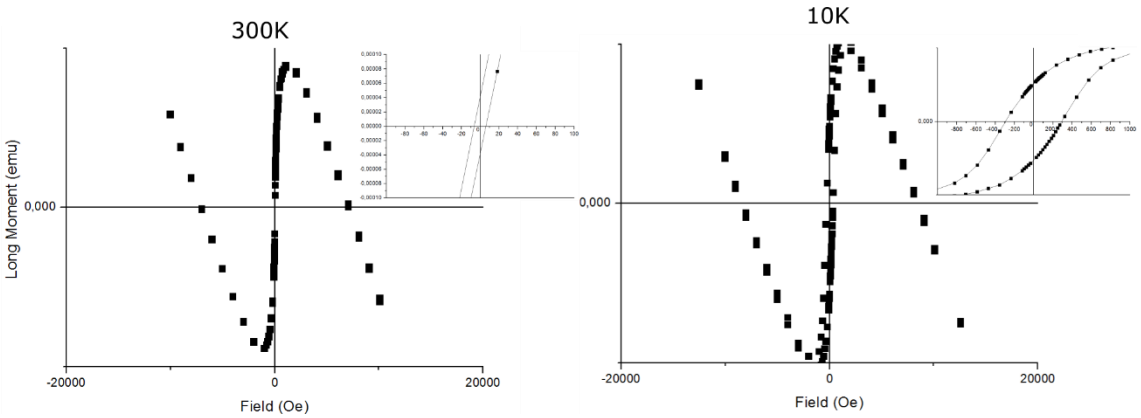


***Figure 22.*** *M(H) SQUID measurements of the synthesized SPION-Paclitaxel-loaded NLCs at 300 K and 10 K, a centered, zoomed version of each (top).*

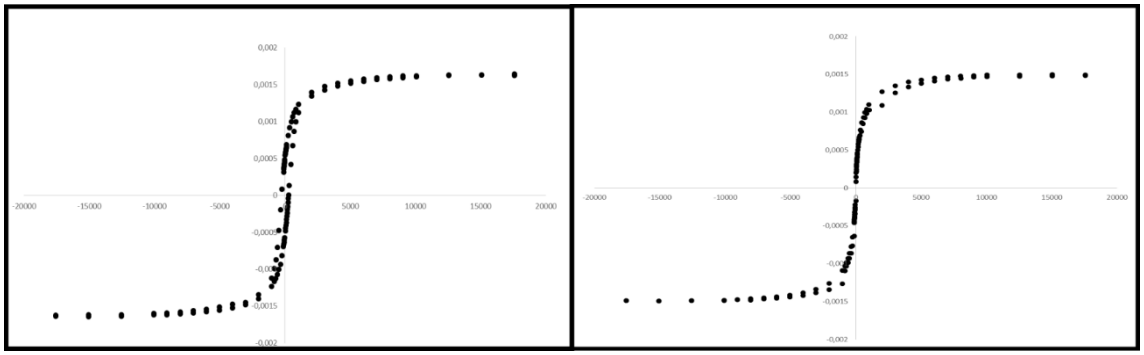

***Figure 23.*** *Corrected values of M(H) SQUID measurements of SPION-Paclitaxel loaded NLCs at 10 K (left) and 300 K (right).*

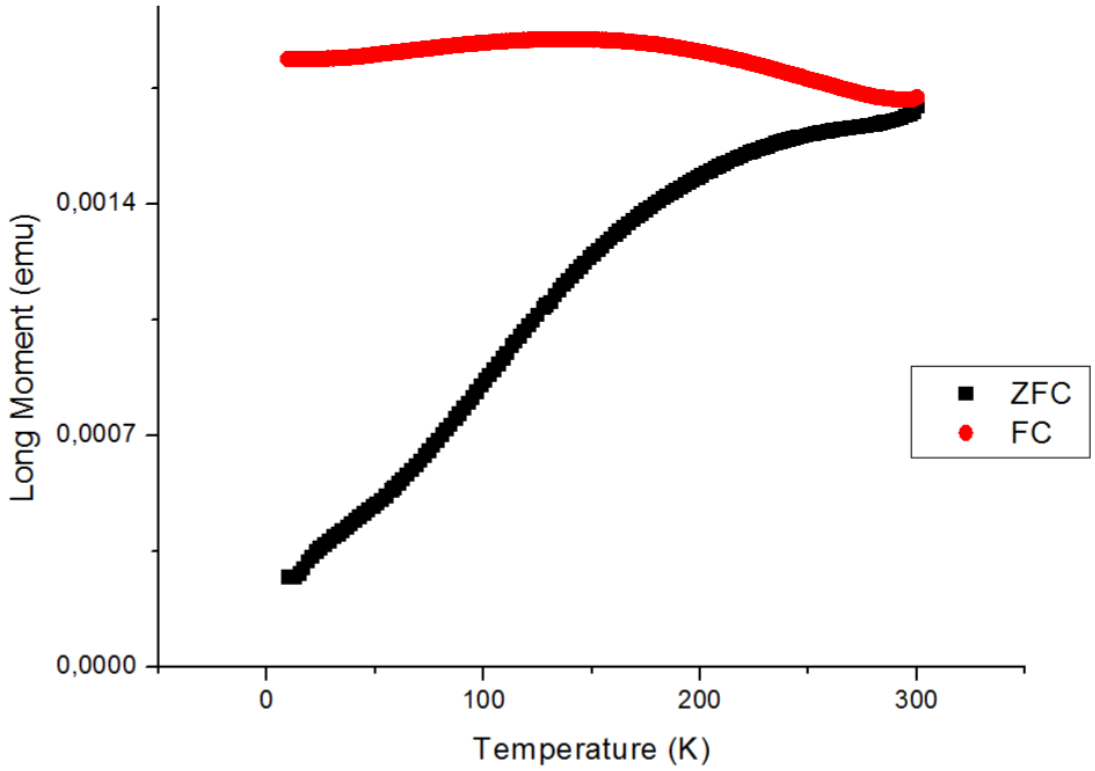


***Figure 24.*** *Zero-Field-Cooled and Field-Cooled measurements of a synthesized SPION-loaded NLC placebo.*

To possibilitate the determination of the SPION's blocking temperature, a SPION-loaded NLC placebo was made, with the aim of decreasing the strong interparticle dipolar interactions and eliminate their influence in the zero-field-cooled and field-cooled measurements (**Figure 24**). This time, the FC curve showed a characteristic elevation, correlated with the successful inhibition of such interactions and the consequent temperature shift. Therefore, it was possible to determine the point of curve juxtaposition present at 300 K, which is associated with the irreversible temperature, the highest blocking temperature of the ensemble [169]. The mean blocking temperature, since the formulation was somewhat polydisperse, was determined through the temperature derivative of the difference between FC and ZFC magnetization curves, to which its maxima corresponds [152]. The calculated mean $T_b$ was, surprisingly, 106.4 K.

An *in vitro* paclitaxel release study was conducted in a simulated physiological and neoplastic environment condition, as pH is regarded, through a dynamic dialysis method. As can be observed in **Figure 25**, the release from nanoparticles in the more acidic medium occurs always at a higher degree than in the physiological condition. It is interesting to consider the two distinct regimes denoted by both release profiles, a particularity from this formulation unlike the common drug-encapsulating nanoparticles, which usually present both regimes in the inverse order. The most likely reason for such is the lack of paclitaxel bound to the particle's surface, wherein most nanoparticles have a fraction of their drug. This surface-bound drug is commonly released in a burst-like fashion, to which the encapsulated drug follows in a controlled and encompassed manner. In this case, the drug-free surface avoids the initial violent release and is demarked by a more stable one followed by a, henceforth denominated, controlled burst.

The first regime lasts 29 hours, during which only 4.7% and 1.6% of cumulative paclitaxel amount was released, in neoplastic and physiological simulated conditions, respectively. This sustained release resulted, mainly, from the rearrangement of the particles' structure due to the rise of temperature.

The second regime takes hold at the $30^{th}$ hour and is prominent until the end of the experiment, 68 hours and 20 minutes after the sample is placed in the sink. During this time, a cumulative amount of 30.6% and 25% of paclitaxel was released at pH 6.3 and 7.4, respectively. The controlled burst release is a result of the continuous weakening and progressive instability of the nanoparticle's physical structure, as it augments its lability over time due to the temperature's close proximity to its melting point, and thereby releases the entrapped drug through a diffusion mediated process.

Relating both conditions to one another, it is possible to ascertain a more pronounced release within the simulated neoplastic environment in absolute value. Akin to such, its rate of increase is slightly higher during both of the regimes.

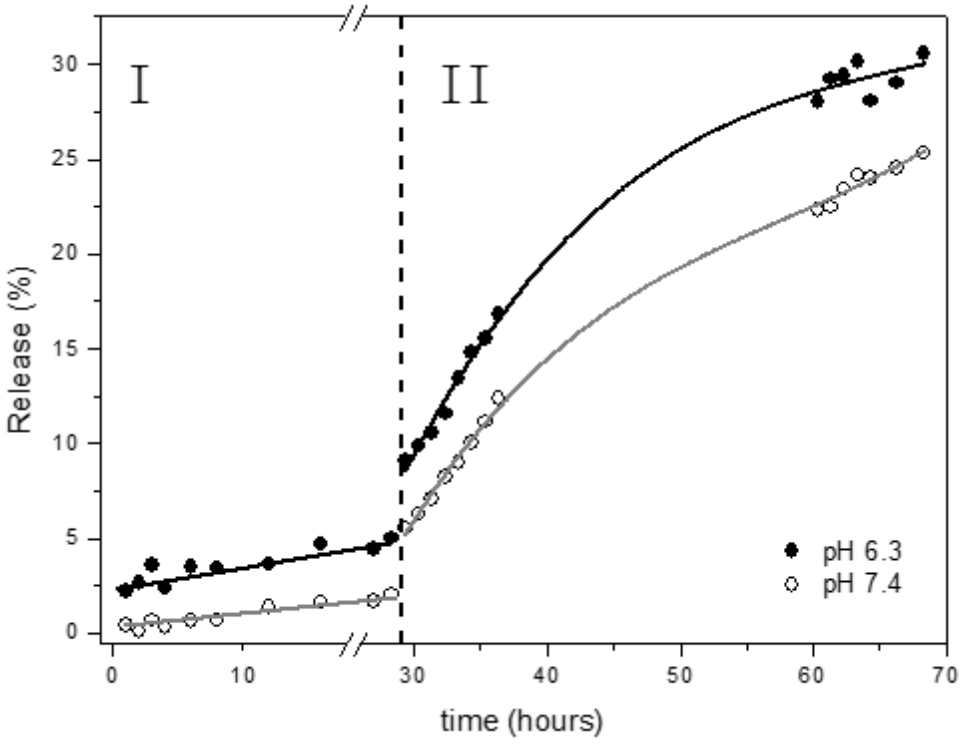


***Figure 25.*** *In vitro paclitaxel release profile from SPION-loaded nanostructured lipid carriers.*

# Chapter 5

## Final remarks

The Paclitaxel-loaded NLC formulation was optimized as intended, presenting a size of 117.83 nm, lower than the 200 nm limit, a polydispersity index of 0.113, indicating monodispersity, and a ζ-potential of -29.2 mV, suggesting a high stability. The encapsulation efficiency achieved was higher than 99%, a value greater than other author had previously reported. The microscopy images were concurrent with the previously measured size and polydispersity index and evidenced a spherical shape.

During the second experimental section, the classical co-precipitation methodology for SPION synthesis was found to be unreliable and lengthy in relation to the more modern microwave-assisted one. The sizing measurements were limited to microscopy imaging since a standard DLS is incapable of identifying such small nanoparticles. The images showed a slightly polydisperse combination of SPIONs averaging 10 nm, indicating a paramagnetic state in concurrence to the initial post-synthesis test with a permanent magnet. The XRD diffraction patterns evidenced a high crystallinity, albeit not disregarding the possible presence of a maghemite phase, representing a good magnetic and structural purity. Magnetization measurements were also conducted, resulting in a virtually null magnetic coercivity at room temperature, evidence of a purely superparamagnetic behavior. The ZFC/FC assays indicated the presence of strong interparticle dipole interactions, due to a horizontal FC curve and pseudo-straight ZFC curve, and the already established slight polydispersity through the changes in the ZFC curve's increase rate at 25 K and 150 K.

Lastly, the optimized Paclitaxel-SPION-loaded NLC formulation was successfully determined through a Box-Behnken design procedure. The resulting formulation was synthesized with a ratio of solid to liquid lipid of 7, 10 mg of Paclitaxel and 15 minutes of sonication, and resulted in a 94.88 nm average nanoparticle with 0.165 polydispersity index and an encapsulation efficiency of 81.14%. The ζ-potential was found to be unaffected by the SPION presence. The images provided by cryomicroscopy denoted a decrease in size and polydispersity as a consequence of the magnetic nanoparticles encapsulation, while no such change is noticeable between the placebo and Paclitaxel-loaded lipid nanoparticles. Additionally, the results were in agreement with the previously measured results by the DLS and evidenced a sphere-like shape. The XRD measured diffraction patterns contained most of the same peaks as the ones obtained from the free SPIONs, with the exception of an obscuration at 18 degrees, most likely caused by the high content of Gelucire® 43/01. In a similar fashion, the magnetization measurements determined a purely superparamagnetic behavior at room temperature resulting from a near zero magnetic coercivity. However, they also presented a slight caveat since, after reaching magnetic saturation, the superparamagnetism of the SPIONs is lost amidst the diamagnetic properties of all the other formulation components. Lastly, the release study indicated an uncommon drug release profile. During the first 29 hours, the sample at pH 6.3 released almost 3-fold the amount of paclitaxel that the sample at pH 7.4 did (4.7% and 1.6%), both following a controlled regime. Afterwards, both samples entered a controlled burst regime,

exponentially increasing the quantity of released drug, amounting to 30.6% and 25% for neoplastic and physiological simulated environment, respectively. These values indicate that the nanoparticle is more prone to release paclitaxel near solid tumors than it is at a healthy tissue.

Overall, this scientific pilgrimage resulted in accomplishment in all three fronts of work. The resulting final formulation is, undoubtedly, a promising candidate for the template of tomorrow's antineoplastic therapies by combining the diminished noxious effects and controlled release property of regular drug-loaded nanoparticle to the hyperthermic capabilities of magnetic nanoparticles, all while creating the additional effect of a burst drug release on-demand.

# Future work

An attempt into science's progress is never finished, as there is always something else to be done.

Specific to this thesis, the logical continuation would be calorimetric assays to precisely and accurately determine the nanoparticle's heating rate, since their superparamagnetic behavior indicates solely that they can heat, not how steeply nor how efficiently. Allied to such, it would be advantageous to verify the relationship between the heating drug releasing properties, such as in a heat-variating release study. Additionally, a more defined stability study is in order, since a time dependent variation (or lack thereof) of nanoparticle diameter and/or ζ-potential represents a more definitive proof than the lack of drug and SPION precipitate in months old formulations. Lastly, cell viability assays need to be conducted in different healthy and neoplastic cell lines under different magnetic field exposures to identify the nanoparticles' cytotoxicity properties in such conditions.

As a final approach, departing from an academic view to a more commercially oriented one, the formulation should also be trialed *in vivo* in animal models and, ultimately, humans.

# References


1. Shinde, N.C., N.J. Keskar, and P.D. Argade, *Nanoparticles: Advances in drug delivery systems.* Res J Pharm Bio Chem Sci, 2012. **3**(1): p. 922-8.
2. Kreuter, J., *Nanoparticles—a historical perspective.* International Journal of Pharmaceutics, 2007. **331**(1): p. 1-10.
3. Hu, K., et al., *Core–shell biopolymer nanoparticle delivery systems: Synthesis and characterization of curcumin fortified zein–pectin nanoparticles.* Food Chemistry, 2015. **182**(0): p. 275-281.
4. Battogtokh, G. and Y.T. Ko, *Self-assembled polymeric nanoparticle of PEGylated chitosan–ceramide conjugate for systemic delivery of paclitaxel.* Journal of Drug Targeting, 2014. **22**(9): p. 813-821.
5. Wang, X., et al., *Delivery of platinum(IV) drug to subcutaneous tumor and lung metastasis using bradykinin-potentiating peptide-decorated chitosan nanoparticles.* Biomaterials, 2014. **35**(24): p. 6439-6453.
6. Kossatz, S., et al., *Efficient treatment of breast cancer xenografts with multifunctionalized iron oxide nanoparticles combining magnetic hyperthermia and anti-cancer drug delivery.* Breast Cancer Research : BCR, 2015. **17**(1): p. 66.
7. Hardiansyah, A., et al., *Magnetic liposomes for colorectal cancer cells therapy by high-frequency magnetic field treatment.* Nanoscale Res Lett, 2014. **9**(1): p. 497.
8. Sano, K., et al., *Markedly Enhanced Permeability and Retention Effects Induced by Photo-Immunotherapy of Tumors.* ACS nano, 2013. **7**(1): p. 717-724.
9. Hu, C.M., et al., *A biomimetic nanosponge that absorbs pore-forming toxins.* Nat Nanotechnol, 2013. **8**(5): p. 336-40.
10. Baac, H.W., et al., *Carbon-nanotube optoacoustic lens for focused ultrasound generation and high-precision targeted therapy.* Sci Rep, 2012. **2**: p. 989.
11. Weis, C., et al., *Labeling of cancer cells with magnetic nanoparticles for magnetic resonance imaging.* Magn Reson Med, 2014. **71**(5): p. 1896-905.
12. Santra, S., *Fluorescent silica nanoparticles for cancer imaging.* Methods Mol Biol, 2010. **624**: p. 151-62.
13. Nam, T., et al., *Tumor targeting chitosan nanoparticles for dual-modality optical/MR cancer imaging.* Bioconjug Chem, 2010. **21**(4): p. 578-82.
14. Gao, X., et al., *In vivo molecular and cellular imaging with quantum dots.* Curr Opin Biotechnol, 2005. **16**(1): p. 63-72.
15. Orndorff, R.L. and S.J. Rosenthal, *Neurotoxin quantum dot conjugates detect endogenous targets expressed in live cancer cells.* Nano Lett, 2009. **9**(7): p. 2589-99.
16. Xu, J., et al., *Comparison of quantum dot technology with conventional immunohistochemistry in examining aldehyde dehydrogenase 1A1 as a potential biomarker for lymph node metastasis of head and neck cancer.* European Journal of Cancer, 2012. **48**(11): p. 1682-1691.
17. Abbas, A., et al., *Hot Spot-Localized Artificial Antibodies for Label-Free Plasmonic Biosensing.* Advanced functional materials, 2013. **23**(14): p. 1789-1797.
18. Halo, T.L., et al., *NanoFlares for the detection, isolation, and culture of live tumor cells from human blood.* Proc Natl Acad Sci U S A, 2014. **111**(48): p. 17104-9.

19. Harris, T.J., et al., *Protease-Triggered Unveiling of Bioactive Nanoparticles.* Small (Weinheim an der Bergstrasse, Germany), 2008. **4**(9): p. 1307-1312.
20. Muthu, M.S., et al., *Nanotheranostics - Application and Further Development of Nanomedicine Strategies for Advanced Theranostics.* Theranostics, 2014. **4**(6): p. 660-677.
21. Maeng, J.H., et al., *Multifunctional doxorubicin loaded superparamagnetic iron oxide nanoparticles for chemotherapy and magnetic resonance imaging in liver cancer.* Biomaterials, 2010. **31**(18): p. 4995-5006.
22. Mieszawska, A.J., et al., *Multifunctional Gold Nanoparticles for Diagnosis and Therapy of Disease.* Molecular Pharmaceutics, 2013. **10**(3): p. 831-847.
23. Kim, D., Y.Y. Jeong, and S. Jon, *A drug-loaded aptamer-gold nanoparticle bioconjugate for combined CT imaging and therapy of prostate cancer.* ACS Nano, 2010. **4**(7): p. 3689-96.
24. Nurunnabi, M., et al., *Targeted near-IR QDs-loaded micelles for cancer therapy and imaging.* Biomaterials, 2010. **31**(20): p. 5436-5444.
25. Etheridge, M.L., et al., *The big picture on nanomedicine: the state of investigational and approved nanomedicine products.* Nanomedicine, 2013. **9**(1): p. 1-14.
26. *World Health Organization - Cancer*. [cited 2015 September]; Available from: http://www.who.int/cancer/en/.
27. Rivera, E., *Liposomal anthracyclines in metastatic breast cancer: clinical update.* Oncologist, 2003. **8 Suppl 2**: p. 3-9.
28. Glantz, M.J., et al., *A randomized controlled trial comparing intrathecal sustained-release cytarabine (DepoCyt) to intrathecal methotrexate in patients with neoplastic meningitis from solid tumors.* Clin Cancer Res, 1999. **5**(11): p. 3394-402.
29. Muggia, F.M., et al., *Phase II study of liposomal doxorubicin in refractory ovarian cancer: antitumor activity and toxicity modification by liposomal encapsulation.* J Clin Oncol, 1997. **15**(3): p. 987-93.
30. Lee, K., et al., *Multicenter phase II trial of Genexol-PM, a Cremophor-free, polymeric micelle formulation of paclitaxel, in patients with metastatic breast cancer.* Breast Cancer Research and Treatment, 2008. **108**(2): p. 241-250.
31. Khemapech, N., et al., *Salvage chemotherapy in recurrent platinum-resistant or refractory epithelial ovarian cancer with Carboplatin and distearoylphosphatidylcholine pegylated liposomal Doxorubicin (lipo-dox(R)).* Asian Pac J Cancer Prev, 2013. **14**(3): p. 2131-5.
32. Rodriguez, M.A., et al., *Vincristine sulfate liposomes injection (Marqibo) in heavily pretreated patients with refractory aggressive non-Hodgkin lymphoma.* Cancer, 2009. **115**(15): p. 3475-3482.
33. Venkatakrishnan, K., et al., *Pharmacokinetics and pharmacodynamics of liposomal mifamurtide in adult volunteers with mild or moderate hepatic impairment.* British Journal of Clinical Pharmacology, 2014. **77**(6): p. 998-1010.
34. Batist, G., et al., *Reduced cardiotoxicity and preserved antitumor efficacy of liposome-encapsulated doxorubicin and cyclophosphamide compared with conventional doxorubicin and cyclophosphamide in a randomized, multicenter trial of metastatic breast cancer.* J Clin Oncol, 2001. **19**(5): p. 1444-54.
35. Rivera Gil, P., et al., *Nanopharmacy: Inorganic nanoscale devices as vectors and active compounds.* Pharmacological Research, 2010. **62**(2): p. 115-125.
36. Chao, Y., et al., *Recognition of dextran-superparamagnetic iron oxide nanoparticle conjugates (Feridex) via macrophage scavenger receptor charged domains.* Bioconjug Chem, 2012. **23**(5): p. 1003-9.
37. FDA. *Feraheme™ (ferumoxytol) Injection Label*. [cited 2015 September]; Available from: http://www.accessdata.fda.gov/drugsatfda_docs/label/2009/022180lbl.pdf.

38. Frank, J.A., et al., *Magnetic intracellular labeling of mammalian cells by combining (FDA-approved) superparamagnetic iron oxide MR contrast agents and commonly used transfection agents.* Acad Radiol, 2002. **9 Suppl 2**: p. S484-7.
39. Wissing, S.A., O. Kayser, and R.H. Müller, *Solid lipid nanoparticles for parenteral drug delivery.* Advanced Drug Delivery Reviews, 2004. **56**(9): p. 1257-1272.
40. Siekmann, B. and K. Westesen, *Submicron-sized parenteral carrier systems based on solid lipids.* Pharm Pharmacol Lett, 1992. **1**: p. 123-6.
41. Pardeike, J., A. Hommoss, and R.H. Müller, *Lipid nanoparticles (SLN, NLC) in cosmetic and pharmaceutical dermal products.* International Journal of Pharmaceutics, 2009. **366**(1–2): p. 170-184.
42. Mehnert, W. and K. Mäder, *Solid lipid nanoparticles: Production, characterization and applications.* Advanced Drug Delivery Reviews, 2001. **47**(2–3): p. 165-196.
43. Müller, R.H., M. Radtke, and S.A. Wissing, *Nanostructured lipid matrices for improved microencapsulation of drugs.* International Journal of Pharmaceutics, 2002. **242**(1–2): p. 121-128.
44. Zhang, X., et al., *PEGylated nanostructured lipid carriers loaded with 10-hydroxycamptothecin: an efficient carrier with enhanced anti-tumour effects against lung cancer.* J Pharm Pharmacol, 2008. **60**(8): p. 1077-87.
45. Patel, A.R., et al., *Efficacy of aerosolized celecoxib encapsulated nanostructured lipid carrier in non-small cell lung cancer in combination with docetaxel.* Pharm Res, 2013. **30**(5): p. 1435-46.
46. Patlolla, R.R., et al., *Formulation, characterization and pulmonary deposition of nebulized celecoxib encapsulated nanostructured lipid carriers.* Journal of Controlled Release, 2010. **144**(2): p. 233-241.
47. How, C.W., et al., *Tamoxifen-loaded nanostructured lipid carrier as a drug delivery system: characterization, stability assessment and cytotoxicity.* Colloids Surf B Biointerfaces, 2013. **112**: p. 393-9.
48. Mussi, S.V., et al., *Improved pharmacokinetics and enhanced tumor growth inhibition using a nanostructured lipid carrier loaded with doxorubicin and modified with a layer-by-layer polyelectrolyte coating.* Int J Pharm, 2015. **495**(1): p. 186-193.
49. Rahman, H.S., et al., *Zerumbone-loaded nanostructured lipid carrier induces G2/M cell cycle arrest and apoptosis via mitochondrial pathway in a human lymphoblastic leukemia cell line.* Int J Nanomedicine, 2014. **9**: p. 527-38.
50. Liu, Q., et al., *Co-delivery of baicalein and doxorubicin by hyaluronic acid decorated nanostructured lipid carriers for breast cancer therapy.* Drug Deliv, 2015: p. 1-5.
51. Ng, W.K., et al., *Thymoquinone-Loaded Nanostructured Lipid Carrier Exhibited Cytotoxicity towards Breast Cancer Cell Lines (MDA-MB-231 and MCF-7) and Cervical Cancer Cell Lines (HeLa and SiHa).* BioMed Research International, 2015. **2015**: p. 263131.
52. Qu, C.Y., et al., *Engineering of lipid prodrug-based, hyaluronic acid-decorated nanostructured lipid carriers platform for 5-fluorouracil and cisplatin combination gastric cancer therapy.* Int J Nanomedicine, 2015. **10**: p. 3911-20.
53. Madane, R.G. and H.S. Mahajan, *Curcumin-loaded nanostructured lipid carriers (NLCs) for nasal administration: design, characterization, and in vivo study.* Drug Deliv, 2015: p. 1-9.
54. Chu, Y., et al., *Preparation and in vitro evaluation of glycyrrhetinic acid-modified curcumin-loaded nanostructured lipid carriers.* Molecules, 2014. **19**(2): p. 2445-57.
55. Zhao, X., et al., *Pharmacokinetics and tissue distribution of docetaxel by liquid chromatography-mass spectrometry: evaluation of folate receptor-targeting amphiphilic copolymer modified nanostructured lipid carrier.* J Chromatogr B Analyt Technol Biomed Life Sci, 2011. **879**(31): p. 3721-7.

56. Yang, X.Y., et al., *Hyaluronic acid-coated nanostructured lipid carriers for targeting paclitaxel to cancer.* Cancer Lett, 2013. **334**(2): p. 338-45.
57. Yuan, Q., et al., *Docetaxel-loaded solid lipid nanoparticles suppress breast cancer cells growth with reduced myelosuppression toxicity.* Int J Nanomedicine, 2014. **9**: p. 4829-46.
58. Jose, S., et al., *In vivo pharmacokinetics and biodistribution of resveratrol-loaded solid lipid nanoparticles for brain delivery.* Int J Pharm, 2014. **474**(1-2): p. 6-13.
59. Athawale, R.B., et al., *Etoposide loaded solid lipid nanoparticles for curtailing B16F10 melanoma colonization in lung.* Biomed Pharmacother, 2014. **68**(2): p. 231-40.
60. Han, Y., et al., *Co-delivery of plasmid DNA and doxorubicin by solid lipid nanoparticles for lung cancer therapy.* Int J Mol Med, 2014. **34**(1): p. 191-6.
61. Zheng, J., et al., *Targeted paclitaxel delivery to tumors using cleavable PEG-conjugated solid lipid nanoparticles.* Pharm Res, 2014. **31**(8): p. 2220-33.
62. Foglietta, F., et al., *Modulation of butyrate anticancer activity by solid lipid nanoparticle delivery: an in vitro investigation on human breast cancer and leukemia cell lines.* J Pharm Pharm Sci, 2014. **17**(2): p. 231-47.
63. Martins, S.M., et al., *Brain targeting effect of camptothecin-loaded solid lipid nanoparticles in rat after intravenous administration.* Eur J Pharm Biopharm, 2013. **85**(3 Pt A): p. 488-502.
64. Zhu, X., et al., *In vitro and in vivo anti-cancer effects of targeting and photothermal sensitive solid lipid nanoparticles.* J Drug Target, 2014. **22**(9): p. 822-8.
65. Tran, T.H., et al., *Hyaluronic acid-coated solid lipid nanoparticles for targeted delivery of vorinostat to CD44 overexpressing cancer cells.* Carbohydr Polym, 2014. **114**: p. 407-15.
66. Venishetty, V.K., et al., *Increased brain uptake of docetaxel and ketoconazole loaded folate-grafted solid lipid nanoparticles.* Nanomedicine, 2013. **9**(1): p. 111-21.
67. Schiff, P.B., J. Fant, and S.B. Horwitz, *Promotion of microtubule assembly in vitro by taxol.* Nature, 1979. **277**(5698): p. 665-667.
68. Rowinsky, E.K., *The development and clinical utility of the taxane class of antimicrotubule chemotherapy agents.* Annu Rev Med, 1997. **48**: p. 353-74.
69. Hamada, H., et al., *Enhancement of water-solubility and bioactivity of paclitaxel using modified cyclodextrins.* Journal of Bioscience and Bioengineering, 2006. **102**(4): p. 369-371.
70. FDA. *Taxol (paclitaxel) injection label*. [cited 2015 September]; Available from: http://www.accessdata.fda.gov/drugsatfda_docs/label/2011/020262s049lbl.pdf.
71. Miele, E., et al., *Albumin-bound formulation of paclitaxel (Abraxane(®) ABI-007) in the treatment of breast cancer.* International Journal of Nanomedicine, 2009. **4**: p. 99-105.
72. Kumar, G.N., et al., *Binding of taxol to human plasma, albumin and alpha 1-acid glycoprotein.* Res Commun Chem Pathol Pharmacol, 1993. **80**(3): p. 337-44.
73. Fellner, S., et al., *Transport of paclitaxel (Taxol) across the blood-brain barrier in vitro and in vivo.* The Journal of Clinical Investigation, 2002. **110**(9): p. 1309-1318.
74. Walle, T., et al., *Taxol metabolism and disposition in cancer patients.* Drug Metab Dispos, 1995. **23**(4): p. 506-12.
75. Campos, F.C., et al., *Systemic toxicity induced by paclitaxel in vivo is associated with the solvent cremophor EL through oxidative stress-driven mechanisms.* Food Chem Toxicol, 2014. **68**: p. 78-86.
76. Gradishar, W.J., *Albumin-bound paclitaxel: a next-generation taxane.* Expert Opin Pharmacother, 2006. **7**(8): p. 1041-53.
77. Yuan, F., et al., *Vascular permeability in a human tumor xenograft: molecular size dependence and cutoff size.* Cancer Res, 1995. **55**(17): p. 3752-6.
78. Cabanes, A., et al., *Comparative in vivo studies with paclitaxel and liposome-encapsulated paclitaxel.* Int J Oncol, 1998. **12**(5): p. 1035-40.

79. Sharma, A., et al., *Activity of paclitaxel liposome formulations against human ovarian tumor xenografts.* Int J Cancer, 1997. **71**(1): p. 103-7.
80. Sharma, A., U.S. Sharma, and R.M. Straubinger, *Paclitaxel-liposomes for intracavitary therapy of intraperitoneal P388 leukemia.* Cancer Lett, 1996. **107**(2): p. 265-72.
81. Sharma, A., E. Mayhew, and R.M. Straubinger, *Antitumor effect of taxol-containing liposomes in a taxol-resistant murine tumor model.* Cancer Res, 1993. **53**(24): p. 5877-81.
82. Cavalli, R., O. Caputo, and M.R. Gasco, *Preparation and characterization of solid lipid nanospheres containing paclitaxel.* European Journal of Pharmaceutical Sciences, 2000. **10**(4): p. 305-309.
83. Arica Yegin, B., J.P. Benoit, and A. Lamprecht, *Paclitaxel-loaded lipid nanoparticles prepared by solvent injection or ultrasound emulsification.* Drug Dev Ind Pharm, 2006. **32**(9): p. 1089-94.
84. Lee, M.-K., S.-J. Lim, and C.-K. Kim, *Preparation, characterization and in vitro cytotoxicity of paclitaxel-loaded sterically stabilized solid lipid nanoparticles.* Biomaterials, 2007. **28**(12): p. 2137-2146.
85. Yuan, H., et al., *Cellular uptake of solid lipid nanoparticles and cytotoxicity of encapsulated paclitaxel in A549 cancer cells.* Int J Pharm, 2008. **348**(1-2): p. 137-45.
86. Dong, X., et al., *Development of new lipid-based paclitaxel nanoparticles using sequential simplex optimization.* Eur J Pharm Biopharm, 2009. **72**(1): p. 9-17.
87. Dong, X., et al., *Doxorubicin and paclitaxel-loaded lipid-based nanoparticles overcome multidrug resistance by inhibiting P-glycoprotein and depleting ATP.* Cancer Res, 2009. **69**(9): p. 3918-26.
88. Koziara, J.M., et al., *Paclitaxel nanoparticles for the potential treatment of brain tumors.* J Control Release, 2004. **99**(2): p. 259-69.
89. Yang, Y., et al., *Preparation and characterization of photo-responsive cell-penetrating peptide-mediated nanostructured lipid carrier.* J Drug Target, 2014. **22**(10): p. 891-900.
90. Yang, Y., et al., *Photo-responsive and NGR-mediated multifunctional nanostructured lipid carrier for tumor-specific therapy.* J Pharm Sci, 2015. **104**(4): p. 1328-39.
91. Kaur, P., et al., *Development, optimization and evaluation of surfactant-based pulmonary nanolipid carrier system of paclitaxel for the management of drug resistance lung cancer using Box-Behnken design.* Drug Deliv, 2015: p. 1-14.
92. Taratula, O., et al., *Nanostructured lipid carriers as multifunctional nanomedicine platform for pulmonary co-delivery of anticancer drugs and siRNA.* J Control Release, 2013. **171**(3): p. 349-57.
93. Araújo, J., et al., *Optimization and physicochemical characterization of a triamcinolone acetonide-loaded NLC for ocular antiangiogenic applications.* International Journal of Pharmaceutics, 2010. **393**(1–2): p. 168-176.
94. M. Demirel, Y.Y.R.H.M.F.K.B.B., *Formulation and in vitro-in vivo evaluation of piribedil solid lipid micro- and nanoparticles.* Journal of Microencapsulation, 2001. **18**(3): p. 359-371.
95. Müller, R., S. Benita, and B. Böhm, *The theory of high-pressure homogenization.*, in *Emulsions and nanosuspensions for the formulation of poorly soluble drugs.* 1998, Medpharm Scientific Publishers: Stuttgart. p. 177-200.
96. Mojahedian, M.M., et al., *A novel method to produce solid lipid nanoparticles using n-butanol as an additional co-surfactant according to the o/w microemulsion quenching technique.* Chem Phys Lipids, 2013. **174**: p. 32-8.
97. Shahgaldian, P., et al., *Para-acyl-calix-arene based solid lipid nanoparticles (SLNs): a detailed study of preparation and stability parameters.* Int J Pharm, 2003. **253**(1-2): p. 23-38.

98. Quintanar-Guerrero, D., et al., *Adaptation and optimization of the emulsification-diffusion technique to prepare lipidic nanospheres.* Eur J Pharm Sci, 2005. **26**(2): p. 211-8.
99. Schubert, M.A. and C.C. Müller-Goymann, *Solvent injection as a new approach for manufacturing lipid nanoparticles – evaluation of the method and process parameters.* European Journal of Pharmaceutics and Biopharmaceutics, 2003. **55**(1): p. 125-131.
100. Cortesi, R., et al., *Production of lipospheres as carriers for bioactive compounds.* Biomaterials, 2002. **23**(11): p. 2283-2294.
101. García-Fuentes, M., D. Torres, and M.J. Alonso, *Design of lipid nanoparticles for the oral delivery of hydrophilic macromolecules.* Colloids and Surfaces B: Biointerfaces, 2003. **27**(2–3): p. 159-168.
102. Brugè, F., et al., *A comparative study on the possible cytotoxic effects of different nanostructured lipid carrier (NLC) compositions in human dermal fibroblasts.* International Journal of Pharmaceutics.
103. Ferreira, M., et al., *Optimization of nanostructured lipid carriers loaded with methotrexate: A tool for inflammatory and cancer therapy.* International Journal of Pharmaceutics, 2015. **492**(1–2): p. 65-72.
104. Mei, Z., et al., *Solid lipid nanoparticle and microemulsion for topical delivery of triptolide.* European Journal of Pharmaceutics and Biopharmaceutics, 2003. **56**(2): p. 189-196.
105. Kržič, M., M. Šentjurc, and J. Kristl, *Improved skin oxygenation after benzyl nicotinate application in different carriers as measured by EPR oximetry in vivo.* Journal of Controlled Release, 2001. **70**(1–2): p. 203-211.
106. Muchow, M., P. Maincent, and R.H. Müller, *Lipid Nanoparticles with a Solid Matrix (SLN®, NLC®, LDC®) for Oral Drug Delivery.* Drug Development and Industrial Pharmacy, 2008. **34**(12): p. 1394-1405.
107. Cho, Y.W., et al., *Hydrotropic agents for study of in vitro paclitaxel release from polymeric micelles.* Journal of Controlled Release, 2004. **97**(2): p. 249-257.
108. Goldstein, J., et al., *Scanning Electron Microscopy and X-ray Microanalysis*. 3rd ed. 2003: Springer US.
109. Xu, C., et al., *Fast nanoparticle sizing by image dynamic light scattering.* Particuology, 2015. **19**: p. 82-85.
110. Sze, A., et al., *Zeta-potential measurement using the Smoluchowski equation and the slope of the current–time relationship in electroosmotic flow.* Journal of Colloid and Interface Science, 2003. **261**(2): p. 402-410.
111. Albanese, A., P.S. Tang, and W.C.W. Chan, *The Effect of Nanoparticle Size, Shape, and Surface Chemistry on Biological Systems.* Annual Review of Biomedical Engineering, 2012. **14**(1): p. 1-16.
112. Clogston, J. and A. Patri, *Zeta Potential Measurement*, in *Characterization of Nanoparticles Intended for Drug Delivery*, S.E. McNeil, Editor. 2011, Humana Press. p. 63-70.
113. Saini, S., et al., *Magnetism: a primer and review.* AJR Am J Roentgenol, 1988. **150**(4): p. 735-43.
114. Likhtenshtein, G.I., et al., *Chapter 1. Fundamentals of Magnetism*, in *Nitroxides: Applications in Chemistry, Biomedicine, and Materials Science*. 2008, Wiley-VCH Verlag GmbH & Co. KGaA. p. 1-45.
115. Reis, M., *Chapter 1 - Introduction*, in *Fundamentals of Magnetism*, M. Reis, Editor. 2013, Academic Press: Boston. p. 2-12.
116. Spicer, D.S., *Magnetic energy storage and the thermal versus non-thermal hard X-ray hypotheses.* Advances in Space Research, 1982. **2**(11): p. 135-137.
117. Reis, M., *Chapter 7 - Diamagnetism*, in *Fundamentals of Magnetism*, M. Reis, Editor. 2013, Academic Press: Boston. p. 74-92.

118. Reis, M., *Chapter 8 - Paramagnetism*, in *Fundamentals of Magnetism*, M. Reis, Editor. 2013, Academic Press: Boston. p. 93-126.
119. Hergt, R., et al., *Physical limits of hyperthermia using magnetite fine particles.* Magnetics, IEEE Transactions on, 1998. **34**(5): p. 3745-3754.
120. Bucak, S., B. Yavuzturk, and A. Demir, *Magnetic Nanoparticles: Synthesis, Surface Modifications and Application in Drug Delivery*, in *Recent Advances in Novel Drug Carrier Systems*. 2012, InTech. p. 167-200.
121. Chen, Q. and Z.J. Zhang, *Size-dependent superparamagnetic properties of MgFe2O4 spinel ferrite nanocrystallites.* Applied physics letters, 1998. **73**: p. 3156.
122. Gutfleisch, O., et al., *Magnetic materials and devices for the 21st century: stronger, lighter, and more energy efficient.* Adv Mater, 2011. **23**(7): p. 821-42.
123. Bañobre-López, M., A. Teijeiro, and J. Rivas, *Magnetic nanoparticle-based hyperthermia for cancer treatment.* Reports of Practical Oncology & Radiotherapy, 2013. **18**(6): p. 397-400.
124. Rudolf, H., et al., *Magnetic particle hyperthermia: nanoparticle magnetism and materials development for cancer therapy.* Journal of Physics: Condensed Matter, 2006. **18**(38): p. S2919.
125. Hiergeist, R., et al., *Application of magnetite ferrofluids for hyperthermia.* Journal of Magnetism and Magnetic Materials, 1999. **201**(1–3): p. 420-422.
126. Gonzales-Weimuller, M., M. Zeisberger, and K.M. Krishnan, *Size-dependant heating rates of iron oxide nanoparticles for magnetic fluid hyperthermia.* Journal of Magnetism and Magnetic Materials, 2009. **321**(13): p. 1947-1950.
127. Rosensweig, R.E., *Heating magnetic fluid with alternating magnetic field.* Journal of Magnetism and Magnetic Materials, 2002. **252**(0): p. 370-374.
128. Gonzalez-Fernandez, M.A., et al., *Magnetic nanoparticles for power absorption: Optimizing size, shape and magnetic properties.* Journal of Solid State Chemistry, 2009. **182**(10): p. 2779-2784.
129. Mornet, S., et al., *Magnetic nanoparticle design for medical diagnosis and therapy.* Journal of Materials Chemistry, 2004. **14**(14): p. 2161-2175.
130. Mahmoudi, M., et al., *Cell toxicity of superparamagnetic iron oxide nanoparticles.* J Colloid Interface Sci, 2009. **336**(2): p. 510-8.
131. Mahmoudi, M., et al., *Toxicity evaluations of superparamagnetic iron oxide nanoparticles: cell "vision" versus physicochemical properties of nanoparticles.* ACS Nano, 2011. **5**(9): p. 7263-76.
132. Massart, R., *Preparation of aqueous magnetic liquids in alkaline and acidic media.* Magnetics, IEEE Transactions on, 1981. **17**(2): p. 1247-1248.
133. Mahmoudi, M., et al., *Optimal Design and Characterization of Superparamagnetic Iron Oxide Nanoparticles Coated with Polyvinyl Alcohol for Targeted Delivery and Imaging†.* The Journal of Physical Chemistry B, 2008. **112**(46): p. 14470-14481.
134. Kang, Y.S., et al., *Synthesis and Characterization of Nanometer-Size Fe3O4 and γ-Fe2O3 Particles.* Chemistry of Materials, 1996. **8**(9): p. 2209-2211.
135. Lopez, R.G., et al., *Chitosan-coated magnetic nanoparticles prepared in one step by reverse microemulsion precipitation.* Int J Mol Sci, 2013. **14**(10): p. 19636-50.
136. Okoli, C., et al., *Comparison and functionalization study of microemulsion-prepared magnetic iron oxide nanoparticles.* Langmuir, 2012. **28**(22): p. 8479-85.
137. Maurizi, L., et al., *One step continuous hydrothermal synthesis of very fine stabilized superparamagnetic nanoparticles of magnetite.* Chem Commun (Camb), 2011. **47**(42): p. 11706-8.
138. Shen, M., et al., *Facile one-pot preparation, surface functionalization, and toxicity assay of APTS-coated iron oxide nanoparticles.* Nanotechnology, 2012. **23**(10): p. 105601.

139. Xu, Y., et al., *Bleomycin loaded magnetite nanoparticles functionalized by polyacrylic acid as a new antitumoral drug delivery system.* Biomed Res Int, 2013. **2013**: p. 462589.
140. Zhu, H., et al., *One-pot solvothermal synthesis of highly water-dispersible size-tunable functionalized magnetite nanocrystal clusters for lipase immobilization.* Chem Asian J, 2013. **8**(7): p. 1447-54.
141. Kumar, R.V., et al., *Fabrication of magnetite nanorods by ultrasound irradiation.* Journal of Applied Physics, 2001. **89**(11): p. 6324-6328.
142. Vijayakumar, R., et al., *Sonochemical synthesis and characterization of pure nanometer-sized Fe3O4 particles.* Materials Science and Engineering: A, 2000. **286**(1): p. 101-105.
143. Khollam, Y.B., et al., *Microwave hydrothermal preparation of submicron-sized spherical magnetite (Fe3O4) powders.* Materials Letters, 2002. **56**(4): p. 571-577.
144. Li, C., et al., *Microwave-solvothermal synthesis of Fe3O4 magnetic nanoparticles.* Materials Letters, 2013. **107**(0): p. 23-26.
145. Osborne, E.A., et al., *Rapid microwave-assisted synthesis of dextran-coated iron oxide nanoparticles for magnetic resonance imaging.* Nanotechnology, 2012. **23**(21): p. 215602.
146. Kappe, C.O., *Controlled Microwave Heating in Modern Organic Synthesis.* Angewandte Chemie International Edition, 2004. **43**(46): p. 6250-6284.
147. Mahdavi, M., et al., *Synthesis, surface modification and characterisation of biocompatible magnetic iron oxide nanoparticles for biomedical applications.* Molecules, 2013. **18**(7): p. 7533-48.
148. Klang, V., C. Valenta, and N.B. Matsko, *Electron microscopy of pharmaceutical systems.* Micron, 2013. **44**: p. 45-74.
149. Harris, K.M., *Powder Diffraction Crystallography of Molecular Solids*, in *Advanced X-Ray Crystallography*, K. Rissanen, Editor. 2012, Springer Berlin Heidelberg. p. 133-177.
150. Skakle, J., *Applications of X-ray powder diffraction in materials chemistry.* Chem Rec, 2005. **5**(5): p. 252-62.
151. Robbes, D., *Highly sensitive magnetometers—a review.* Sensors and Actuators A: Physical, 2006. **129**(1–2): p. 86-93.
152. Pereira, C., et al., *Superparamagnetic MFe2O4 (M = Fe, Co, Mn) Nanoparticles: Tuning the Particle Size and Magnetic Properties through a Novel One-Step Coprecipitation Route.* Chemistry of Materials, 2012. **24**(8): p. 1496-1504.
153. Pereira, A.M., et al., *Unravelling the effect of interparticle interactions and surface spin canting in γ-Fe2O3@SiO2 superparamagnetic nanoparticles.* Journal of Applied Physics, 2011. **109**(11): p. 114319.
154. Welch, M.J., C.J. Hawker, and K.L. Wooley, *The Advantages of Nanoparticles for PET.* Journal of Nuclear Medicine, 2009. **50**(11): p. 1743-1746.
155. Müller, R.H., et al., *Cytotoxicity of magnetite-loaded polylactide, polylactide/glycolide particles and solid lipid nanoparticles.* International Journal of Pharmaceutics, 1996. **138**(1): p. 85-94.
156. Babincová, M., et al., *AC-magnetic field controlled drug release from magnetoliposomes: design of a method for site-specific chemotherapy.* Bioelectrochemistry, 2002. **55**(1–2): p. 17-19.
157. Béalle, G., et al., *Ultra Magnetic Liposomes for MR Imaging, Targeting, and Hyperthermia.* Langmuir, 2012. **28**(32): p. 11834-11842.
158. Gonzales, M. and K.M. Krishnan, *Synthesis of magnetoliposomes with monodisperse iron oxide nanocrystal cores for hyperthermia.* Journal of Magnetism and Magnetic Materials, 2005. **293**(1): p. 265-270.

159. Pang, X., et al., *Preparation and characterization of magnetic solid lipid nanoparticles loaded with ibuprofen.* Asian Journal of Pharmaceutical Sciences, 2009. **4**(2): p. 132-137.
160. Igartua, M., et al., *Development and characterization of solid lipid nanoparticles loaded with magnetite.* International Journal of Pharmaceutics, 2002. **233**(1–2): p. 149-157.
161. Hsu, M.H. and Y.C. Su, *Iron-oxide embedded solid lipid nanoparticles for magnetically controlled heating and drug delivery.* Biomed Microdevices, 2008. **10**(6): p. 785-93.
162. Box, G.E. and D.W. Behnken, *Some new three level designs for the study of quantitative variables.* Technometrics, 1960. **2**(4): p. 455-475.
163. Gidwani, B. and A. Vyas, *Preparation, characterization, and optimization of altretamine-loaded solid lipid nanoparticles using Box-Behnken design and response surface methodology.* Artif Cells Nanomed Biotechnol, 2014: p. 1-10.
164. Maleki Dizaj, S., et al., *Application of Box-Behnken design to prepare gentamicin-loaded calcium carbonate nanoparticles.* Artif Cells Nanomed Biotechnol, 2015: p. 1-7.
165. Wang, F., et al., *Optimization of methazolamide-loaded solid lipid nanoparticles for ophthalmic delivery using Box-Behnken design.* J Liposome Res, 2014. **24**(3): p. 171-81.
166. Yerlikaya, F., et al., *Development and evaluation of paclitaxel nanoparticles using a quality-by-design approach.* J Pharm Sci, 2013. **102**(10): p. 3748-61.
167. Wallace, S., et al., *Drug release from nanomedicines: selection of appropriate encapsulation and release methodology.* Drug Delivery and Translational Research, 2012. **2**(4): p. 284-292.
168. Modi, S. and B.D. Anderson, *Determination of Drug Release Kinetics from Nanoparticles: Overcoming Pitfalls of the Dynamic Dialysis Method.* Molecular Pharmaceutics, 2013. **10**(8): p. 3076-3089.
169. Proenca, M.P., et al., *Size and surface effects on the magnetic properties of NiO nanoparticles.* Physical Chemistry Chemical Physics, 2011. **13**(20): p. 9561-9567.